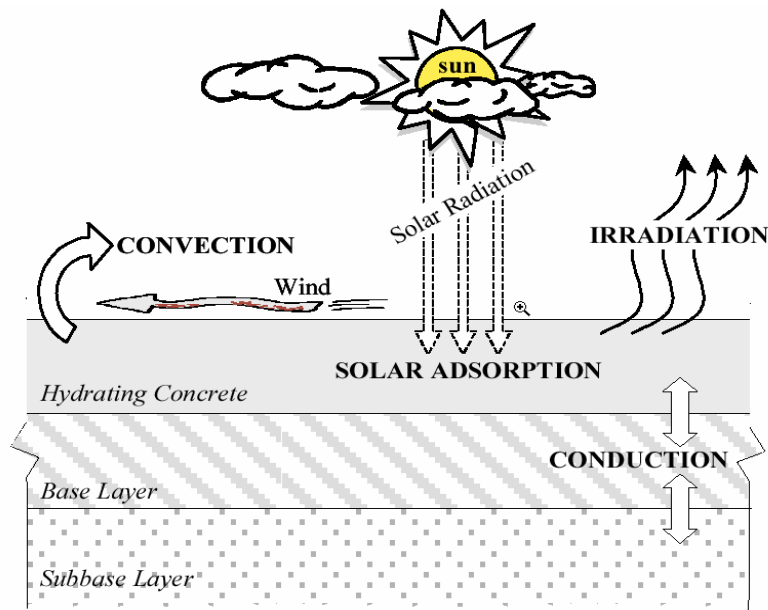An **IPRF** Research Report

Innovative Pavement Research Foundation
Airport Concrete Pavement Technology Program

Report IPRF 01-G-002-04-2(s)   **Characterization and Analysis of Early Age Concrete Pavement Behavior at the National Airport Pavement Test Facility (NAPTF)**

\

Programs Management Office
5420 Old Orchard Road
Skokie, IL 60077   **August 2007(r)**

An *IPRF* Research Report

Innovative Pavement Research Foundation
Airport Concrete Pavement Technology Program

Report IPRF 01-G-002-04-2(s)   **Characterization and Analysis of Early Age Concrete Pavement Behavior at the National Airport Pavement Test Facility (NAPTF)**

Prepared by

Texas Transportation Institute
3135 TAMU
College Station, Texas 77843-3135

Principal Investigators

Dan Ye, Graduate Research Assistant
Texas Transportation Institute
Texas A&M University

Dr. Dan G. Zollinger, P.E.
Texas Transportation Institute
Texas A&M University

Contributing Author

Mr. Dennis A. Morian, P.E.
Quality Engineering Solutions, Inc.

PREFACE

This report has been prepared by the Innovative Pavement Research Foundation (IPRF) under the Airport Concrete Pavement Technology Program. Funding is provided by the Federal Aviation Administration (FAA) under Cooperative Agreement Number 01-G-002-04-2. Dr. Satish Agrawal is the Manager of the FAA Airport Technology R&D Branch and the Technical Manager of the Cooperative Agreement. Mr. Jim Lafrenz is the IPRF Cooperative Agreement Program Manager.

TABLE OF CONTENTS

LIST OF FIGURES

Page

LIST OF TABLES

1. INTRODUCTION

1.1 PURPOSE

The primary objective for this research effort is as follows:

To monitor, characterize, and analyze the early-age concrete pavement behavior.

To fulfill this objective, three sub objectives were identified as follows:

1. *On-site testing* – concrete moisture measurements, set maturity determination, and drying shrinkage monitoring.

2. *Early-age concrete temperature and moisture modeling* – the temperature and moisture history of early-age concrete play an important role in the strength development of concrete. Furthermore, internal strains due to temperature and moisture gradients cause concrete slab curling and warping. This modeling couples the temperature and moisture fields together in a finite element (FEM) program called Temperature and Moisture Analysis for Curing Concrete (TMAC^2).

3. *Field data analysis* – field acquired temperature and moisture data were used to calibrate thermal conductivity and moisture diffusivity coefficients. The backcalculated thermal conductivity and moisture diffusivity were used to forward calculate temperature and moisture gradients. Set maturity was used to determine the set temperature and set moisture gradients. Nonlinear temperature and moisture gradients were transformed into equivalent linear gradients for mechanical analysis purposes.

1.2 BACKGROUND

The early-age concrete temperature and moisture history is of great importance for concrete strength development (Powers 1947; Neville 1996). The internal strains due to temperature and moisture gradients cause curling and warping of a concrete slab, which is of great interest as far as the performance of the pavement is concerned. As such, the modeling of early-age concrete temperature and moisture is becoming an essential element of pavement design analysis. The Texas Transportation Institute (TTI) is one of the leading agencies that excel in early-age concrete properties. The software TMAC^2 developed at TTI is capable of characterizing the coupled temperature and moisture fields in early-age concrete, which facilitate pavement engineers' efforts to carry out mechanistic pavement design analysis.

2. ON-SITE TESTING

2.1 INTRODUCTION

A full scale concrete test pavement was cast at the FAA National Airport Pavement Test Facility (NAPTF) near Atlantic City, New Jersey to investigate the performance of a two-layer unbonded concrete pavement structure with variable thicknesses. TTI was asked to assist in monitoring of the on-site curing history and characterization of early-age concrete behavior. To establish a material baseline, penetration testing (ASTM C 803 1999) and free shrinkage testing (ASTM C 157 1999) were conducted on-site. Measurements and tests conducted by TTI are listed below:

- ➢ Relative humidity monitoring in three sections,
- ➢ Penetration testing, and
- ➢ Free shrinkage testing.

2.2 STRUCTURAL CONFIGURATION OF THE TEST SECTIONS

A matrix consisting of three structural configurations was constructed. These sections were 9" on 6" (section 1), 7.5" on 7.5" (section 2), and 6" on 10" (section 3) as shown in Figure 1. The total thickness of each concrete overlay section is 15". A nominal one inch asphalt bond breaker was placed between the concrete layers of each section so that the assumption of relatively unbonded conditions between the layers can be established.

2.3 INSTRUMENTATION AND TEST SETUP

A curing Monitor System (CMS), manufactured by A-Tek Co. in Dallas, TX, was used to monitor relative humidity at three different vertical locations (above the surface of the slab, on the surface of the slab, and 1 inch below the surface of the slab). A detailed view of all the sensors is shown in Figure 2. The CMS device has three relative humidity sensors to measure ambient relative humidity, concrete surface humidity and concrete relative humidity, respectively. The concrete RH sensor is of the chilled mirror hydrometer type, which is sometimes called an optical condensation hygrometer. This is considered to be the most accurate, reliable, and fundamental hygrometer commercially available. As a result, it is widely used as a calibration standard for other types of relative humidity sensors. Since the environment inside young concrete is highly saturated, the chilled mirror hygrometer is well configured to measure the relative humidity under these conditions. Recent versions of the CMS include the capacity to monitor wind speed and solar radiation, which are another two important factors affecting evaporation and curing quality. Those two sensors are also shown in Figure 3.

Relative humidity measurements at the concrete surface and inside the concrete require sampling chambers in order to equalize the measured water vapor pressure with that inside the concrete pores. The chamber for the chilled mirror sensor is inserted 1 inch

into the concrete. The chamber for concrete surface humidity rests on the surface of the fresh concrete (but below the curing compound) where it consists of a filter disk which serves as a top cover to the sampling chamber and to which a layer of curing compound is sprayed. This configuration creates a sufficiently large sampling volume with which to measure the humidity of the concrete surface. With this configuration the relative humidity in the surface chamber represents the humidity of the concrete surface immediately below the curing membrane.

Test procedure ASTM C803 (1999) *Standard Test Method for Penetration Resistance of Hardened Concrete* was conducted to determine the initial and final set of the on-site concrete mix. The test set up is shown in Figure 4.

A vibrating wire gage EM-5 (Figure 5) was used to measure the free shrinkage strain (ASTM C 157 1999), which is a volumetric internal strain due to moisture loss. A relative humidity measurement was taken within the same specimen in order to establish the relationship between moisture content (relative humidity) and shrinkage. The test setup is shown in Figure 6.

2.4 DATA PRESENTATION

Results from penetration, free shrinkage and relative humidity monitoring are presented in this section. These results are used to determine the final concrete set maturity, establish the relationship between free shrinkage and relative humidity, and to carry out an assessment of curing quality.

2.4.1 Penetration Test

A penetration specimen was prepared on February 27th, but due to the low temperature conditions at the site, the concrete strength development was delayed until the first day after placement. All penetration resistance data points were obtained in the second day after concrete placement. According to the specifications (ASTM C 803 1999), the resistance values for initial and final set are 450 psi and 4000 psi respectively. The resulting initial set maturity was 295 $^\circ$C-hr and the final set maturity was 395 $^\circ$C -hr. The penetration test results relating penetration resistance and concrete maturity are presented in Figure 7.

2.4.2 Free Shrinkage Test

The ASTM C 157 (1999) procedure was employed to measure the shrinkage due to moisture loss. A relative humidity sensor was inserted in the specimen to acquire moisture data and a vibrating wire gage was embedded inside the specimen so that the correlation between relative humidity and shrinkage could be established. This relationship appeared to be linear based on the regressed test results with an r-squared of 0.97.

2.4.3 Relative Humidity Data

Four sets of curing data were obtained: those for the lower layer and upper layer surfaces in section 1, and for the lower layer and upper layer surfaces in section 2. The allocation of the sections is shown in Figure 1. A Type I (transparent type) curing compound was spayed about 45 minutes after concrete placement. After final set, a small amount of water was sprayed on the concrete surface to keep the concrete moist, after which plastic sheets were used to cover the concrete pavement surface.

For each set of curing data, relative humidity data at three different locations, potential of evaporation (PE) (ACI 305R 1999), and evaporation rate (ER) were determined. Equations (1) and (2) are used to calculate PE and ER respectively. PE serves as an indicator of the ambient weather severity of evaporation potential. ER is the actual evaporation rate from the concrete surface, which includes the effects of PE, concrete moisture condition, concrete maturity, and the curing compound effectiveness.

$$PE = \left[T_c^{2.5} - \left(RH_a \cdot T_a^{2.5} \right) \right] \left(1 + 0.4 \cdot WS \right) \times 10^{-6} \tag{1}$$

where,

PE $\quad$ = Potential of Evaporation, $lb/ft^2/hr$

T_s $\quad$ = Concrete Surface Temperature, $^{\circ}F$,

T_a $\quad$ = Air Temperature, $^{\circ}F$,

RH_a $\quad$ = (Ambient Relative Humidity %) / 100, and

WS $\quad$ = Wind Velocity, mph

$$ER = \frac{a \cdot PE \cdot wc \cdot RH_s}{\left(1 + b \cdot Maturity^c \right) \left(1 + ECT \right)^d} \tag{2}$$

where,

a, b, c, d $\quad$ = regression parameters , and

wc $\quad$ = water cementitious ratio.

$$Maturity = \sum \beta_T \beta_{RH} \cdot \Delta t \tag{3}$$

where,

β_T = $(T - T_0)$, $T_0 = 10\ ^{\circ}C$, and

β_{RH} = $1/(1 + (7.5 - 7.5 \cdot RH_s)^4)$ (Bažant and Najjar 1972)

$$ECT = \frac{Ln\left(RH_s / RH_a \right)}{\left(RH_c - RH_s \right)} \tag{4}$$

where,

RH_c $\quad$ = concrete relative humidity, and

RH_s $\quad$ = concrete surface relative humidity.

As has been observed many times before, the relative humidity of the freshly placed concrete started low and then built up over time. During these early stages the diffusivity

of the concrete is so high that the water vapors can not build up for several hours but eventually do begin to increase as the concrete matures. The surface relative humidity remained nearly constant (around 80%) in all four instances. This can be accredited to the use of plastic sheeting for cure protection. Experience from several field tests where the curing medium consisted of only curing compound indicates that the surface relative humidity reduces significantly during the second day after concrete placement and tends to follow the trends of the ambient relative humidity, thereafter. Relative humidity is the ratio of the water vapor pressure divided by the saturated vapor pressure. Therefore, the relative humidity changes inversely with the air temperature.

Due to the indoor environment in which the concrete was placed, the ambient relative humidity trends were not observed to be entirely normal for a pavement placement, but reached the lowest point at approximately noon when the ambient temperature was the highest, and began to increase as the ambient temperature decreased. This ambient relative humidity cycling phenomenon can be attributed to the fact that the moisture capacity of air is dependent on the air temperature. Air at a higher temperature has greater capacity to hold water vapor, however inside the NAPTF facility the amount of water vapor in the air for the most part remained unchanged through out the day. The relative humidity is the ratio of the water vapor pressure divided by the saturated vapor pressure. Therefore, the relative humidity changes inversely with the air temperature.

Low ambient relative humidity, high wind speed, high temperature and high solar radiation create conditions conducive to a high rate of evaportation. Normally for outside placements, the worst combination occurs during the afternoon hours. Placement of the concrete inside the NAPTF facility eliminated the influence of wind and solar radiation. The air temperature was around 40 °F to 50 °F during the lower layer placement and 45°F to 70°F during the upper layer placement. Due to these conditions, low PE was experienced as shown in Figure 10, Figure 12, Figure 14, and Figure 16. Even lower values of ERs were expected with the use of plastic sheets. The measured ERs diminished quickly as the concrete matured since the resulting low diffusivity of matured concrete served to protect the concrete even further from moisture loss.

2.5 SUMMARY

A low curing temperature delayed the concrete setting. Curing was very good due to the use of plastic sheeting since the surface humidity was maintained above 80%. In all cases, the potential for evaporation was less than 0.04 lbs/ft^2/hr, which represents very mild curing conditions. Good curing (plastic sheeting) and mild ambient conditions (low PE) both ensured sufficient moisture inside the concrete for adequate hydration.

3. EARLY-AGE CONCRETE TEMPERATURE AND MOISTURE MODELING

3.1 INTRODUCTION

This chapter integrates models for early age concrete heat and moisture transport into one product. Thermal conductivity and moisture diffusivity were determined as functions of concrete temperature, concrete moisture and degree of hydration, which is important because the temperature and moisture analysis is nonlinear. Since temperature and moisture vary primarily in the vertical direction, a one dimensional simplification was adopted.

3.2 THEORY FOR CONCRETE AGING

The strength of concrete is a function of its age, temperature history and most probably the moisture history (Bažant 1970; Buch and Zollinger 1993). The technique for estimating the strength development of concrete based on temperature history is the maturity method (ASTM C 1074 1999). The equivalent age described in equation (5) is an important concept.

$$t_e = \int_0^t \beta_T \beta_{RH} dt \qquad (5)$$

where β_T and β_{RH} are the weighting factors determined according to the concrete temperature and moisture conditions. Equation (6) is one of the many models for β_T, which was suggested by Freiesleben Hansen and Pederson (Freiesleben Hansen and Pederson 1977) based on the Arrhenius equation.

$$\beta_T = \exp\left(-\frac{E}{R}\left(\frac{1}{273+T} - \frac{1}{273+T_r}\right)\right) \qquad (6)$$

where
T = concrete temperature, $^\circ$C
T_r = reference temperature, $^\circ$C,
E = activation energy, J/mol, and
R = universal gas constant, 8.3144 J/(mol K).
β_{RH} is shown in equation (7) (Bažant 1970).

$$\beta_{RH} = \frac{1}{1+(a-aRH)^b} \qquad (7)$$

where RH is the concrete relative humidity, and a, b are adjustable coefficients. Bažant (Bažant 1970) assigned a = 7.5 and b = 4, while Jeong (2003) reported that a = 5 and b =1 had better prediction based on the strength data he obtained. The illustration of β_{RH} vs. RH is shown in Figure 17.

Degree of hydration α can be expressed as either: the current strength over the ultimate strength, the hydrated cementious materials over the total cementious materials, or the heat generated over the total heat etc. It can be characterized by equation (8):

$$\alpha(t_e) = \alpha_u \cdot \exp\left(-\left(\tau/t_e\right)^\beta\right) \qquad (8)$$

where

α_u = ultimate degree of hydration,

τ = hydration time parameter, hrs, and

β = hydration shape parameter.

These parameters can be determined from the information about the mixture design. The heat generation rate and self-desiccation rate are dependants of the derivative of the degree of hydration with respect to time. The derivative is presented in equation (9):

$$\frac{\partial \alpha}{\partial t} = \frac{\left(\tau/t_e\right)^\beta \beta_T \beta_{RH} \alpha}{t_e} \qquad (9)$$

3.3 CONCRETE TEMPERATURE

Concrete temperature is controlled mostly by the ambient weather conditions and the concrete thermal conductivity. For early age concrete, the hydration process also affects the concrete temperature. Figure 18 illustrates the factors that affect concrete temperature.

3.3.1 Governing Equation

From the perspective of conservation of energy, the governing equation for heat transfer inside a concrete body is formulated in equation (10).

$$div \cdot \left(K \cdot grad(T)\right) + Q = \rho c \dot{T} \qquad (10)$$

where

K = thermal conducivity,

Q = heat generation rate by hydration,

ρ = concrete density, and

c = specific heat.

From the definition of degree of hydration, the heat generated by hydration can be obtained from equation (7).

$$H = H_u \cdot \alpha(t_e) \qquad (11)$$

where H_u is the total heat that can be generated and H is the heat actually generated. In order to get the heat generation rate, equation (11) was used to obtain the first derivative with respect to time. The resulting heat generation rate was obtained as shown in equation (12).

$$Q = dH\!\!\diagup\!\!dt = H_u \cdot \frac{(\tau/t_e)^{\beta} \beta_T \beta_{RH} \alpha}{t_e} \tag{12}$$

3.3.2 Boundary Conditions

3.3.2.1 Convection

Heat energy can be transferred from a slab surface to the surrounding environment by wind currents. This heat transfer is facilitated by random molecular motion in the atmosphere. In other words, convection heat transfer occurs between the wind flow and the surface of a concrete slab when they are at different temperatures. If the temperatures between the slab surface and the wind flow differ, temperature in the wind current above the slab will vary from T_s at the slab surface to T_a in the air flow above the slab surface. Convection heat transfer is expressed as (Says and Crawford 1980; Kaviany 1994):

$$q''_{conv} = h_c \left(T_s - T_a \right) \tag{13}$$

where q''_{conv} (W/m^2) is the convective heat flux and h_c (W/m^2/K) is the convective heat transfer coefficient. The convective heat transfer coefficient is affected by many variables. An empirical formula is used to relate convection heat transfer coefficient to wind velocity and roughness of slab surface (Branco, Mendes et al. 1992).

$$h_c = 6 + 3.7v \tag{14}$$

where 6 W/m^2/K represents an average slab surface roughness without wind effects. The heat transfer coefficient increases proportionally with an increase in wind speed.

3.3.2.2 Irradiation

Irradiation transfers heat energy by electromagnetic waves while conduction and convection require a material medium. Emissive power E (W/m^2) indicates the rate of heat energy release from the surface of a concrete slab per unit area through irradiation transfer. The upper limit of emissive power is shown as (Incropera and DeWitt 1996):

$$E = \varepsilon \sigma T_s^4 \tag{15}$$

where, T_s (K) is the absolute temperature at the surface of a concrete slab and σ (=5.67×10-8 W/m^2/K^4) is the Stafan-Boltzmann constant. The term ε is the emissivity,

which ranges from 0 to 1. It is a radioactive property of the slab surface and provides a measure of how efficiently the surface emits energy relative to a blackbody. Irradiation for a concrete pavement is determined from the concept that a slab surface at temperature T_s is radiating to a much larger surface at temperature T_a surrounding the slab surface. Irradiation heat transfer can be expressed as (Meinel and Meinel 1976; Siegel and Howell 1981):

$$q_r^{''} = \varepsilon\sigma\left(T_s^4 - T_a^4\right) \tag{16}$$

3.3.2.3 Solar Radiation

Solar radiation ($q_s^{''}$) absorbed directly into a concrete slab surface causes the surface of the slab to be heated more rapidly than the interior region. This effect contributes to a temperature gradient through the depth of the slab (Hsieh, Qin et al. 1989; Branco, Mendes et al. 1992). There are several factors which influence the solar radiation absorption into a given slab surface. These include the time of the day and year, the latitude, and cloudiness, and so on (Chapman 1982; Taljaston 1987; Branco, Mendes et al. 1992). Solar radiation consists of direct and indirect components. The direct component is the direct solar radiation that is directly incident on the surface while the indirect radiation refers to the indirect solar radiation resulting from multiple scattering by the environment. Accordingly, the total solar radiation that reaches the surface of a concrete slab is the sum of direct and indirect contributions (Branco, Mendes et al. 1992):

$$q_s^{''} = \alpha\left[I_d \sin\theta + I_i\left(\frac{1 + \cos\gamma}{2}\right)\right] \tag{17}$$

where
$q_s^{''}$ = solar radiation (W/m^2)
α = surface heat absorptivity of concrete (= 0.6) (Chapman 1982)
I_d = direct solar radiation (W/m^2)
I_i = indirect solar radiation (W/m^2)
θ = incident angle of solar radiation against the slab surface (degree)
γ = inclination angle of slab surface (degree)

The amount of solar radiation received by the slab surface depends on the incident angle of solar radiation against the slab surface and the inclination angle of the slab surface. The incident angle of solar radiation can be determined by a method presented by Hsieh et al.(Hsieh, Qin et al. 1989). The indirect solar radiation may range from 10% of the total solar radiation on a clear day to nearly 100% on a totally sunny day. No solar radiation absorption occurs at night since the sun rays are no longer present.

3.3.2.4 Heat Flux Due to Evaporation.

Including heat flux due to evaporation in the boundary condition of heat transfer at the slab top surface is important to accurately account for moisture effects on the temperature conditions at the surface of a concrete pavement. Few temperature prediction models consider the evaporation effects in their boundary conditions (Kapila, Falkowsky et al. 1997). There have been many efforts to develop concrete temperature prediction models which can be easily used although they ignore the effect of heat flux due to evaporation in their boundary conditions(Yang 1996; Ruiz, Schindler et al. 2001). Heat flux due to evaporation can be calculated by:

$$q_e^{''} = EH_v \tag{18}$$

where

E = rate of evaporation (kg/m^2/h or W/m^3)
Hv = heat of vaporization of water

$= 597.3 - 0.564T_s$ (cal/g)

$= 427(597.3 - 0.564T_s)$ (m)

3.4 CONCRETE MOISTURE

3.4.1 Moisture Diffusion

Concrete moisture diffusion can be characterized by the law of conservation of moisture mass as shown in equation (19). The term on the left side states the moisture content change rate inside any point of a medium while the first term on the right side represents the moisture content change due to moisture transport and the second term on the right side characterizes the moisture content change due to self-desiccation.

$$\frac{\partial \theta}{\partial t} = div(c \cdot grad(RH)) + \frac{\partial \theta_s}{\partial t} \tag{19}$$

where
θ = volumetric water content, g/cm^3,
c = moisture conductivity, g/(cm·sec),
θs = hydrated volumetric water, g/cm^3, and
RH = relative humidity.

Using the chain rule, equation (19) is rewritten as:

$$\frac{\partial RH}{\partial t} = \frac{\partial RH}{\partial \theta} div(c \cdot grad(RH)) + \frac{\partial RH}{\partial \theta} \frac{\partial \theta_s}{\partial t} \tag{20}$$

10

where $\dfrac{\partial RH}{\partial \theta}$ is known as moisture capacity, which is further discussed later. Applying the concept of degree of hydration again, degree of hydration could be expressed as:

$$\alpha = \frac{\theta_s}{\theta_u} \tag{21}$$

where θ_u is the total water needed for complete hydration. So equation (20) can be further revised as:

$$\frac{\partial RH}{\partial t} = \frac{\partial RH}{\partial \theta} div\big(c \cdot grad(RH)\big) + \frac{\partial RH}{\partial \theta} \frac{\partial \theta_s}{\partial \alpha} \frac{\partial \alpha}{\partial t} \tag{22}$$

where $\dfrac{\partial \theta_s}{\partial \alpha}$ is a constant for a certain type of concrete mixture and $\dfrac{\partial \alpha}{\partial t}$ is given in equation (12). The boundary condition of moisture transport is presented as (Bažant and Najjar 1972):

$$J = B \ln(RH_s - RH_a) \tag{23}$$

where B is the emissivity of the concrete surface, RH_s is the surface relative humidity and RH_a is the ambient relative humidity.

3.4.2 Moisture Capacity.

The relationship between humidity and water content within concrete at a constant temperature and the degree of hydration is described by desorption or sorption isotherms (Bažant and Najjar 1972). It is evident that the relationship between the moisture and the measured humidity of the concrete will vary as a function of age. The dependence of the evaporable water content on humidity (as a function of temperature) is a function of the porosity of the pore structure within the cement paste and is represented empirically in the form of desorption or sorption isotherms as illustrated in Figure 19. It should be noted that the isotherm for sorption is different from the isotherm for desorption. This characteristic may be due to the various states of equilibrium of the pore water and the effect of surface energy, which applies forces in different directions when the concrete is in desorption or sorption state. An investigation by Parrott (Parrott 1988) implied the significance of porosity with respect to the position of the desorption or sorption isotherm within concrete. The results indicated that a greater amount of moisture loss in drying concrete would occur in regions nearest to exposed drying surfaces which may be also regions of greater porosity. Therefore, it can be explained that there is a greater volume of coarse pores at positions nearer to an exposed concrete surface and consequently the relationship between weight loss and relative humidity of concrete will vary with distance from the exposed surface. In this respect, the performance and behavior of a concrete pavement may be affected by the porosity of the surface. It should also be noted that the resulting desorption isotherm at any time during hydration of a hardening concrete slab

11

must be interpreted not only as a function of the degree of hydration, but also as a function of porosity. At a given porosity, the desorption isotherm may be expressed in the differential form as (Bažant and Najjar 1972) $dH = kdw$, where dH is the change of relative humidity, dw is the change of volumetric water content, and k is known as moisture capacity. Xi, Bažant, and Jennings (Xi, Bažant et al. 1994) developed a model to characterize the cementitious material moisture capacity.

3.5 FEM FORMULATION

The finite element method is a very powerful tool for solving differential equations based on variational principles. Since the temperature and moisture distributions in concrete are mostly dependent on the depth, modeling can be simplified by assuming one-dimensional flow.

3.5.1 FEM Variational Derivation.

The one dimensional variation formulation of equation (10) is:

$$\int \left[\frac{d}{dx}\left(K\frac{dT}{dx} \right) + Q - \rho c \dot{T} \right] \delta T dx = 0 \tag{24}$$

By integrating by parts, equation (24) becomes:

$$\int \left[-K\frac{dT}{dx}\delta\left(\frac{dT}{dx} \right) + Q\delta T - \rho c \dot{T}\delta T \right] dx + K\frac{dT}{dx}\delta T \bigg|_{x=a}^{x=b} = 0 \tag{25}$$

T is approximated by the following equation:

$$T = T_i^m N_i \tag{26}$$

where N_i is the approximation function and T_{im} is the nodal temperature at time step m. The approximation of T in the time dimension can be expressed as a forward finite difference formulation. So equation (26) becomes:

$$\int \left[KN_{ix}N_{jx} \right] dx T_j^m + \frac{\int \rho c N_i N_j dx T_j^{m+1} - \int \rho c N_i N_j dx T_j^m}{\Delta t} = \int QN_j dx \tag{27}$$

where N_{ix} means the first derivative of N_i with respect to x and Δt is the time interval. It should be noticed that K and Q in the above equation are not constant throughout the integration domain. For the boundary terms all the external heat at the boundary node should be added to the right side of equation (27) in accordance with the node number. To obtain the FEM formulae for moisture diffusion, the same process needs to be followed. The one dimensional variational formulation of equation (18) is given by equation (28).

$$\int \left[\frac{\partial RH}{\partial \theta} \cdot \frac{d}{dx}\left(c\frac{dRH}{dx} \right) + \frac{\partial RH}{\partial \theta}\frac{\partial \theta_s}{\partial \alpha}\frac{\partial \alpha}{\partial t} - \frac{\partial RH}{\partial t} \right] \delta RH\, dx = 0 \qquad (28)$$

Integrating by parts, equation (28) becomes:

$$\int \left[\begin{array}{l} -\dfrac{\partial RH}{\partial \theta}\, c\, \dfrac{dRH}{dx}\, \delta\!\left(\dfrac{dRH}{dx}\right) - \dfrac{\partial^2 RH}{\partial \theta\, \partial x}\, c\, \dfrac{dRH}{dx}\, \delta RH \\[2ex] + \dfrac{\partial RH}{\partial \theta}\dfrac{\partial \theta_s}{\partial \alpha}\dfrac{\partial \alpha}{\partial t}\, \delta RH - \dfrac{dRH}{dt}\, \delta RH \end{array} \right] dx$$
$$+ \frac{\partial RH}{\partial \theta}\, D\, \frac{dRH}{dx}\, \delta RH \bigg|_{x=a}^{x=b} = 0 \qquad (29)$$

Since the moisture capacity is a function of x, the resulting diffusivity matrix becomes nonsymmetrical. RH is approximated by the following equation.

$$RH = RH_i^m N_i \qquad (30)$$

where N_i is the approximation function and RH^i_m is the nodal relative humidity at time step m.

Again using the forward difference method to approximate the first derivative of RH with respect to time and substituting $\dfrac{\partial RH}{\partial \theta}c$ with D, which is diffusivity (cm^2/sec), equation (29) can be expressed as follows.

$$\int \left[DN_{ix}N_{jx} + \frac{\partial^2 RH}{\partial \theta\, \partial x}c N_i N_{jx} \right] dx\, RH_j^m$$
$$+ \frac{\int N_i N_j dx\, RH_j^{m+1} - \int N_i N_j dx\, RH_j^m}{\Delta t} = \int \frac{\partial RH}{\partial \theta}\frac{\partial \theta_s}{\partial \alpha}\frac{\partial \alpha}{\partial t} N_j dx \qquad (31)$$

3.5.2 Shape functions and matrix formulation

Shape functions are the basic functions to approximate the primary variables. Quadratic functions are used as shape functions. Figure 20 illustrates a one-dimension quadratic element with a length of 2a. The shape functions are presented in equation (32). Figure 21 shows the plots of the shape functions.

$$N_1 = \frac{1}{2a^2} x(x - a)$$

$$N_2 = -\frac{1}{a^2}(x + a)(x - a) \qquad (32)$$

$$N_3 = \frac{1}{2a^2} x(x + a)$$

It is observed from equation (27) and (31) that there are four types of integration to be evaluated.

$$\int_{-a}^{a} U N_{ix} N_{jx} dx \qquad (33)$$

$$\int_{-a}^{a} U N_i N_j dx \qquad (34)$$

$$\int_{-a}^{a} U N_j dx \qquad (35)$$

$$\int_{-a}^{a} U N_i N_{jx} dx \qquad (36)$$

where U is a dummy term and a function of x. For example, U is replaced by K in order to evaluate the first term of equation (27). For simplicity, U is approximated by shape functions as well.

$$U = U_i N_i \qquad (37)$$

Ui is evaluated at each node. The explicit form of equation (33) is given as a matrix in equation (38).

$$\begin{bmatrix} \dfrac{1}{60}\dfrac{37U_1 + 36U_2 - 3U_3}{a} & -\dfrac{1}{15}\dfrac{11U_1 + 8U_2 + U_3}{a} & \dfrac{1}{60}\dfrac{7U_1 - 4U_2 + 7U_3}{a} \\ -\dfrac{1}{15}\dfrac{11U_1 + 8U_2 + U_3}{a} & \dfrac{4}{15}\dfrac{3U_1 + 4U_2 + 3U_3}{a} & -\dfrac{1}{15}\dfrac{U_1 + 8U_2 + 11U_3}{a} \\ \dfrac{1}{60}\dfrac{7U_1 - 4U_2 + 7U_3}{a} & -\dfrac{1}{15}\dfrac{U_1 + 8U_2 + 11U_3}{a} & -\dfrac{1}{60}\dfrac{3U_1 - 36U_2 - 37U_3}{a} \end{bmatrix} \qquad (38)$$

The U term in equation (34) is constant throughout the integrating domain. As a result, equation (34) can be expressed as a simpler matrix as shown in equation (39).

$$
U \begin{bmatrix} \dfrac{4}{15}a & \dfrac{2}{15}a & -\dfrac{1}{15}a \\[2mm] \dfrac{2}{15}a & \dfrac{16}{15}a & \dfrac{2}{15}a \\[2mm] -\dfrac{1}{15}a & \dfrac{2}{15}a & \dfrac{4}{15}a \end{bmatrix} \tag{39}
$$

The right sides of equation (24) and (31) can be evaluated by equation (40).

$$
\begin{bmatrix} \dfrac{1}{15}a(4U_1 + 2U_2 - U_3) \\[2mm] \dfrac{2}{15}a(U_1 + 8U_2 + U_3) \\[2mm] \dfrac{1}{15}a(-U_1 + 2U_2 + 4U_3) \end{bmatrix} \tag{40}
$$

Equation (36) gives a non-symmetric matrix as shown in equation (41).

$$
\begin{bmatrix} -\dfrac{1}{3}U_1 - \dfrac{1}{5}U_2 + \dfrac{1}{30}U_3 & \dfrac{2}{5}U_1 + \dfrac{4}{15}U_2 & -\dfrac{1}{15}U_1 - \dfrac{1}{15}U_2 - \dfrac{1}{30}U_3 \\[2mm] -\dfrac{1}{5}U_1 - \dfrac{8}{15}U_2 + \dfrac{1}{15}U_3 & \dfrac{4}{15}U_1 - \dfrac{4}{15}U_3 & -\dfrac{1}{15}U_1 + \dfrac{8}{15}U_2 + \dfrac{1}{5}U_3 \\[2mm] \dfrac{1}{30}U_1 + \dfrac{1}{15}U_2 + \dfrac{1}{15}U_3 & -\dfrac{4}{15}U_2 - \dfrac{2}{5}U_3 & -\dfrac{1}{30}U_1 + \dfrac{1}{5}U_2 + \dfrac{1}{3}U_3 \end{bmatrix} \tag{41}
$$

3.6 SUMMARY

This section synthesizes current models for conducting early age concrete temperature and moisture analysis. As the maturation of concrete is an aging phenomenon, the thermal conductivity and moisture diffusivity are variable as concrete matures. The moisture capacity concept was used to characterize the water movement by means of relative humidity. With this integrated knowledge at hand, the FEM formulae were derived. These formulae are very useful for conducting mechanistic analysis of pavement behavior.

4. TMAC^2 ANALYSIS

4.1 INTRODUCTION

In section 2, relative humidity data related to curing effectiveness and other concrete properties, i.e. initial and final set maturity and the relation between shrinkage and relative humidity, were reported. In this section, thermal conductivity and moisture diffusivity are backcalculated from the temperature and moisture data obtained from section 3, which consisted of a 10" bottom layer and 6" top layer. With the temperature conductivity and moisture diffusivity information, TMAC^2, a finite element program previously described, was used to forward calculate temperature and moisture gradients through the depth of the concrete pavement. After conducting the TMAC^2 analysis, temperature and moisture gradient history, set temperature and moisture gradient can be used to simulate curling and warping behavior of a concrete slab.

4.2 TMAC^2 ANALYSIS

As previously noted, the TMAC^2 program is a set of dedicated finite element analysis software products developed by TTI to simulate temperature and moisture variations for concrete pavement slabs. Its capability includes a module to backcalculate the material properties (thermal conductivity and moisture diffusivity) from measured data in addition to capturing the coupling effect of thermal and moisture transport particularly during early age hardening.

4.2.1 Hydration Parameters

The water cement ratio of the concrete was 0.50. Hydration parameters listed in Table 1 are selected based on the water cement ratio and the type of cement. The aging of concrete is characterized by equation (8).

4.2.2 Ambient Conditions

Ambient temperature, ambient relative humidity, wind speed and solar radiation are four main factors that affect the temperature and moisture distribution inside concrete pavement. The test road was cast inside the NAPTF facilities; therefore wind speed and solar radiation were assigned zeros for the TMAC^2 analysis. Ambient temperature and relative humidity were modeled as sine functions for each day. The recorded average daily high and low ambient temperature and relative humidity are presented in Table 2. The highest temperature occurred at 2:00 PM each day and the relative humidity followed the inverse trend of the ambient temperature. The ambient temperature and relative humidity for the two testing periods are plotted in Figure 22 and Figure 23 respectively.

4.2.3 Thermal Conductivity and Moisture Diffusivity

Concrete thermal conductivity and moisture diffusivity are believed to be functions of the state of concrete temperature, relative humidity and degree of hydration. The following equations (42) and (43) are the proposed models for the thermal conductivity and moisture diffusivity.

$$K = (a - b\alpha)(0.0212T + 0.5321)(1.25RH^2 + 0.25RH + 0.5) \qquad (42)$$

where,
K   = thermal conductivity, J/(cm·hr·°C),
a, b= adjustable coefficients,
α = degree of hydration,
T   = temperature, °C, and
RH= relative humidity.

$$D = (c - d\alpha)(0.0212T + 0.5321)(1.25RH^2 + 0.25RH + 0.5) \qquad (43)$$

where,
D   = moisture diffusivity, cm^2/hr, and
c, d= adjustable coefficients.

The coefficients a, b, c, and d are adjusted by fitting the TMAC^2 predicted concrete temperature and relative humidity results to the measured concrete temperature and relative humidity data. The calibrated coefficients are listed in Table 3.

Figure 24, Figure 25, and Figure 26 shows how degree of hydration, temperature, and relative humidity affect concrete thermal conductivity (K) and moisture diffusivity (D). As concrete matures, the concrete porosity decreases: as a result the moisture diffusivity decreases. The decrease of thermal conductivity due to concrete aging can be explained by the decreasing moisture diffusivity and its mitigating effect on the transfer of heat. As temperature increases, both thermal conductivity and moisture diffusivity increase similar to the case when RH is increasing.

From Figure 24 (T=20°C and RH=0.9), it is observed that as the degree of hydration increases the thermal conductivity drops from 33 J/cmhr°C to 24 J/cmhr°C, and moisture diffusivity drops from 4.6×10^{-7} to 0.3×10^{-7} cm^2/hr. Figure 25 (α=0.5 and RH=0.9) shows that thermal conductivity increases from 30 J/cmhr°C to 55 J/cmhr°C and the moisture diffusivity increases from 2.5×10^{-7} to 5.0×10^{-7} cm^2/hr with the temperature increasing from 20°C to 60°C. Figure 26 (α=0.5 and T=20°C) shows the effect of RH on thermal conductivity and moisture diffusivity. With RH changing from 0.2 to 1.0, the thermal conductivity increases from 8 J/cmhr°C to 33 J/cmhr°C, and the moisture diffusivity increases from 0.8×10^{-7} cm^2/hr to 3×10^{-7} cm^2/hr. Using adjusted K and D values, the comparison between the predicted temperature history and measured temperature histories at different locations are presented in Figure 27, Figure 28, and Figure 29.

It is observed that, during the first day following placement the concrete temperature was so low there was hardly any hydration. As very little hydration heat was generated, the concrete temperature stayed low during the first 20 hours. As the hydration occurred, the concrete temperature began to increase due to the heat that was generated by hydration. The predicted temperatures at three different depths match very well with the measured the concrete temperatures.

The comparisons at measured locations within the slabs between predicted concrete relative humidity and measured concrete relative humidity are presented in Figure 30, Figure 31, and Figure 32. The concrete relative humidity, measured by chilled mirrors, started off low even though the concrete was still in a fresh state and possibly in a saturated condition. However, as the concrete matures the diffusivity decreases and the vapor pressure increases raising the relative humidity. The chilled mirror sensors utilize an electronic heating and cooling system to maintain a constant reading on the dew point temperature of the concrete. The predicted RH at three different depths matches very well with the measured concrete RH as shown in Figure 30, Figure 31, and Figure 32.

4.2.4 Temperature and Moisture Gradients

With known concrete thermal conductivity and moisture diffusivity, temperature and moisture analysis can be predicted for other conditions and sections where measurements were not conducted.

The section configurations are shown in Figure 1. The bottom layers were cast on 2/27/2006 and 2/28/2006; while the top layers were cast on 3/28/2006. The predicted concrete temperature and RH gradients are shown in Figure 33 through Figure 44.

It is observed that the thicker the pavement the larger temperature and moisture gradients and the greater the maximum temperature. For the bottom layers, the maximum temperatures for each section were 12.2 ℃, 13 ℃ and 15.8 ℃ respectively, noting that their thicknesses were 6", 7.5", and 10" respectively. For top layers, the maximum temperatures for each section are 27.5 ℃, 26 ℃ and 23 ℃ respectively while their thicknesses were 9", 7.5", and 6", respectively.

The drying of concrete is accredited to two mechanisms: one is the water movement from the concrete to its adjacent medium (top: water evaporates into the air; bottom: water is sucked into a less saturated base), the other is self-desiccation (the water reduction due to hydration lowers the internal relative humidity). Therefore, the concrete at the surface and bottom are subjected to both kinds of drying mechanisms and the concrete in the middle is subjected mainly to self-desiccation.

The relative humidity for the top layers was decreasing faster than that of the bottom layers. This is because the top layers were cast under relatively warmer ambient conditions which accelerated the hydration process and the self-desiccation.

18

4.2.5 Set Temperature and Moisture Gradient

As reported in section 2, the final set maturity was 395 $^{\circ}$C –hr. Before final set, the concrete was still in a semi-plastic form, so temperature and moisture gradient would effectively not result in the generation of stress. After final set, the concrete slab can be considered rigid enough to produce stress and to respond to temperature and moisture gradient induced stresses. Therefore, the actual effective temperature and moisture gradient is the sum of the forward calculated temperature and moisture gradients offset by the set temperature and moisture gradients. The set temperature and relative humidity gradients are presented in Figure 45 through Figure 50.

The concrete set temperatures were higher for thicker pavements. For the bottom layers, the maximum set temperatures were 9.3 ºC, 9.6ºC, and 10ºC respectively from section 1 to section 3 (thicknesses: 6", 7.5", and 10"); while for the top layers, the maximum set temperatures were 26 ºC, 21ºC, and 19.5ºC respectively from section 1 to section 3 (thicknesses: 9", 7.5", and 6"). The concrete set RH gradients show that thinner pavement had larger set moisture gradients.

4.2.6 Equivalent Linear Temperature and Moisture Gradients.

Temperature and moisture gradients through the depth of the concrete pavement were highly nonlinear. It was, however, necessary to transform these nonlinear gradients into equivalent linear gradients in order to facilitate curling and warping analysis. The transformation follows in the following equations(Mohamed and Hansen 1997):

$$\Delta T_{eq} = -\frac{12M^*}{\alpha h^2} \tag{44}$$

where,
ΔT_{eq} = equivalent linear temperature gradient, °C,
h = slab thickness, m,
α = PCC CTE, m/m/°C, and
M^* = constant dependent on the temperature distribution expressed as shown in the equation (45):

$$M^* = \int_{-h/2}^{h/2} \varepsilon(z) z dz \tag{45}$$

where,
z = distance from slab midplane (z is positive downward), m, and
$\varepsilon(z)$ = strain profile, m/m.

The strain profile is determined by equation (46):

$$\varepsilon(z) = \alpha\left(T_z - T_{z,set}\right) \tag{46}$$

where,

T_z = current temperature at slab depth z, °C, and
$T_{z,set}$ = temperature at slab depth z, at time of set, °C.

Temperature gradient is assumed to be third order polynomial equation as shown in equation (47).

$$T_z = A + Bz + Cz^2 + Dz^3 \qquad (47)$$

where,
A, B, C, and D = coefficients.

Equation (48) can be obtained from the above equations.

$$\Delta T_{eq} = -12\left(\frac{Bh}{12} + \frac{Dh^3}{80}\right) \qquad (48)$$

The same procedure is followed to calculate the equivalent linear moisture gradient, except that B and D are the coefficients for moisture profiles.

The equivalent linear temperature and moisture gradients are calculated based on the above equations and the results are listed in Table 4 through Table 9.

4.3 SUMMARY

This section utilizes the temperature and moisture gradients obtained from the actual measurements conducted at NAPTF to characterize the concrete thermal conductivity and moisture diffusivity. Then, further analysis was carried out to calculate the temperature and moisture gradients in all other sections. Set temperature and moisture gradients were calculated based on the set maturity. Equivalent linear temperature and moisture gradients were calculated for further mechanical analysis purposes.

5. SUMMARY AND CONCLUSIONS

This research has successfully demonstrated the procedures used to monitor, characterize, and evaluate early-age concrete pavement temperature and moisture related behaviors. On-site measurements were conducted to obtain the set maturity vs. moisture-shrinkage relationship. Temperature and moisture profiles measurements from one section were used to calibrate the thermal conductivity and moisture diffusivity models. Measured temperature and moisture gradients match very well with calculated gradients. Based on the calibrated concrete properties, thermal conductivity and moisture diffusivity, forward TMAC^2 calculations were carried out to acquire temperature and moisture gradients for the test sections.

Set temperature gradients, set moisture gradients, and equivalent linear gradients were calculated for slab analysis purposes under environmentally induced loading.

6. REFERENCES

ACI 305R (1999). Hot Weather Concreting, ACI International.

ASTM C 157 (1999). Standard Test Method for Length Change of Hardened Hydraulic-Cement Mortar and Concrete. ASTM. West Conshohocken, PA.

ASTM C 803 (1999). Standard Test Method for Penetration Resistance of Hardened Concrete. ASTM. West Conshohocken, PA.

ASTM C 1074 (1999). Standard Practice for Estimating Concrete Strength by the Maturity Method. ASTM West Conshohocken, PA.

Bažant, Z. P. (1970). "Constitutive Equation for Concrete Creep and Shrinkage Based on Thermodynamics of Multiphase Systems." Materials and Structures **3**(13).

Bažant, Z. P. and L. J. Najjar (1972). "Nonlinear Water Diffusion in Nonsaturated Concrete." Materials and Structures **5**(25).

Branco, F. A., R. A. Mendes, et al. (1992). "Heat of Hydration Effects in Concrete Structures." ACI Materials Journal **89**(2).

Buch, N. and D. G. Zollinger (1993). Preliminary Investigation on Effects of Moisture on Concrete Pavement Strength and Behavior. Transportation Research Board, Washington, D.C., National Research Council.

Chapman, A. J. (1982). Fundamentals of Heat Transfer. New York, NY, Macmillan Inc.

Freiesleben Hansen, P. and J. Pederson (1977). "Maturity computer for controlled curing and hardening of concrete." Nordisk Betong **1**: 19-34.

Hsieh, C. K., C. Qin, et al. (1989). Development of Computer Modeling for Prediction of Temperature Distribution inside Concrete Pavements. Gainesville, FL, Department of Mechanical Engineering, University of Florida.

Incropera, F. P. and D. P. DeWitt (1996). Fundamentals of Heat and Mass Transfer. New York, John Wiley & Sons.

Jeong (2003). Characterization of Slab Behavior and Related Material Properties due to Temperature and Moisture Civil Engineering. College Station, Tx, Texas A&M University. Ph.D.

Kapila, D., J. Falkowsky, et al. (1997). "Thermal Effects During the Curing of Concrete Pavements." ACI Materials Journal **94**(2).

Kaviany, M. (1994). Principles of Convective Heat Transfer. New York, NY, Springer-Verlag.

Meinel, A. B. and M. P. Meinel (1976). Applied Solar Energy: An Introduction. Reading, MA, Addison-Wesley.

Mohamed, A. R. and W. Hansen (1997). "EFFECT OF NONLINEAR TEMPERATURE GRADIENT ON CURLING STRESS IN CONCRETE PAVEMENTS." Transportation Research Board **1568**.

Neville, A. M. (1996). Properties of Concrete. New York, John Wiley and Sons.

Parrott, L. J. (1988). "Moisture Profiles in Drying Concrete." Advances in Cement Research **1**(3).

Powers, T. C. (1947). A Discussion of Cement Hydration in relation to the Curing of Concrete. Highway Resourse Board, Washington D. C.

Ruiz, J. M., A. K. Schindler, et al. (2001). <u>Concrete Temperature Modeling and Strength Prediction Using Maturity Concepts in the FHWA HIPERPAV Software</u>. Proceedings 7th International Conference on Concrete Pavements, Orlando, FL.

Says, W. M. and M. E. Crawford (1980). <u>Convective Heat and Mass Transfer</u>. New York, NY, McGraw-Hill.

Siegel, R. and J. R. Howell (1981). <u>Thermal Radiation Heat Transfer</u>. New York, NY, McGraw-Hill.

Taljaston, B. (1987). Temperature Development and Maturity Growth for Ordinary Swedish Portland Cement Type II. <u>Diploma Work 1987:035</u>. Stockholm, Sweden, Technical University of Lulea.

Xi, Y., Z. P. Bažant, et al. (1994). " Moisture Diffusion in Cementious Materials." <u>Advanced Cement Based Materials</u> **1**.

Yang, S. (1996). A Temperature Prediction Model in New Concrete Pavement and New Test Method for Concrete Fracture Parameters. <u>Department of Civil Engineering</u>. College Station, Texas, Texas A&M University. Ph.D.

Figure 1 Diagram of Concrete Pavement Configuration.

Wind Speed Sensor

Solar Radiation Sensor

Ambient RH Sensor

Surface RH Sensor

Concrete RH Sensor

Curing Monitor System

Sectio
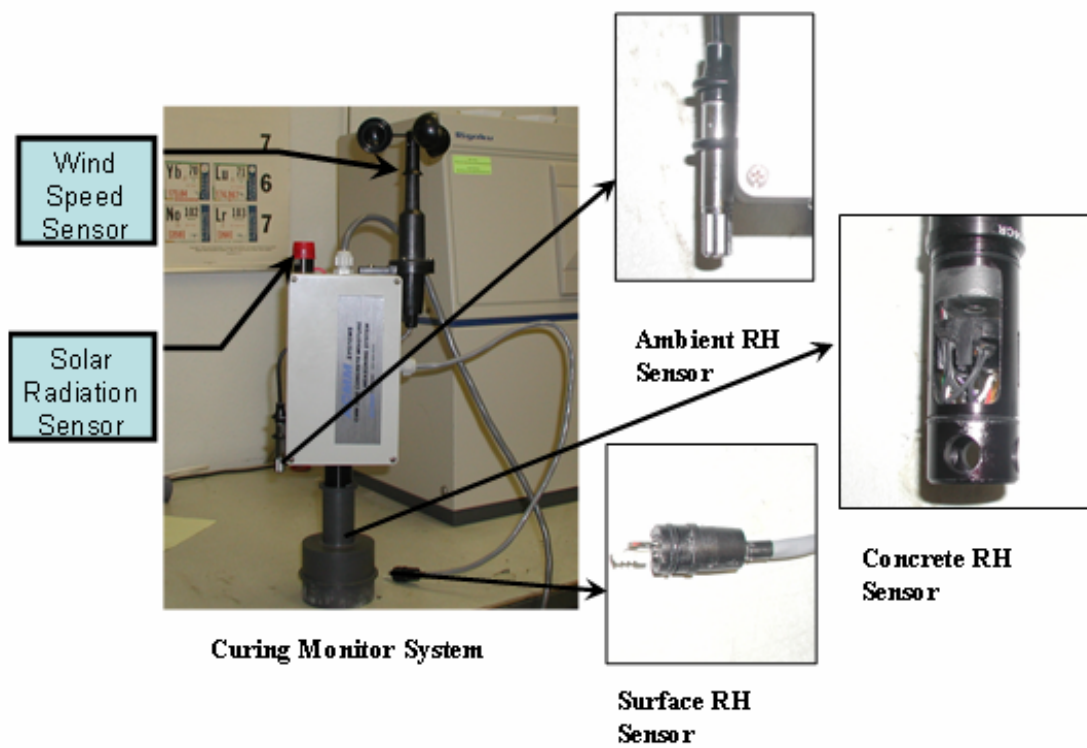
9 in.

6 in.

Figure 2 CMS and its Sensors.

Figure 3 On-site CMS Setup.

Figure 4 Penetration Test Setup.

Figure 5 Vibrating Wire Gage EM-5.

Figure 6 Free Shrinkage Test Setup.
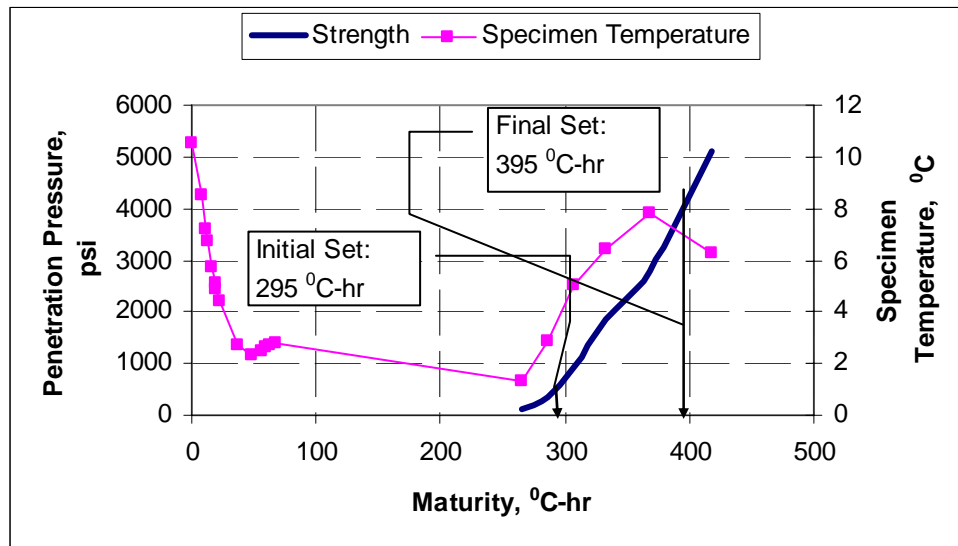
Figure 7 Penetration Test Results.
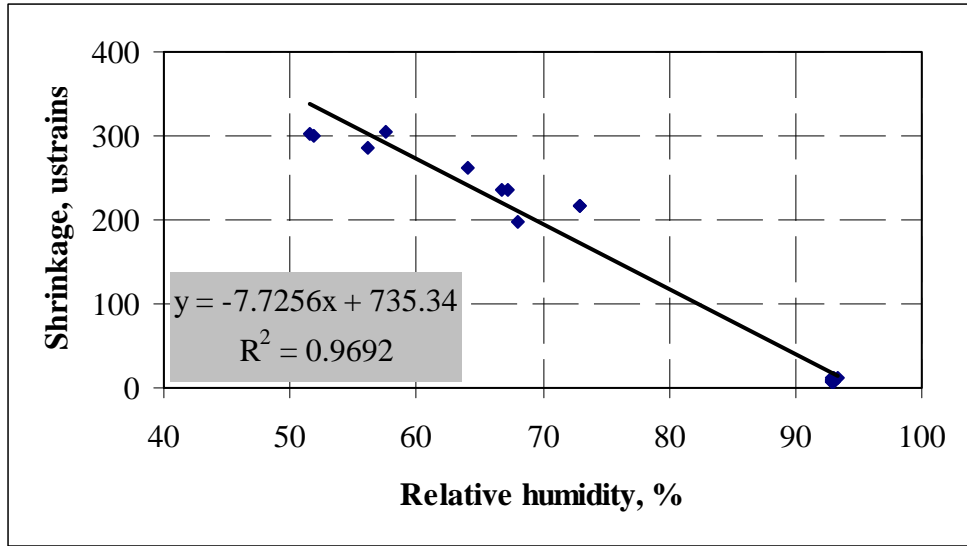
Figure 8 Free Shrinkage vs. Relative Humidity.
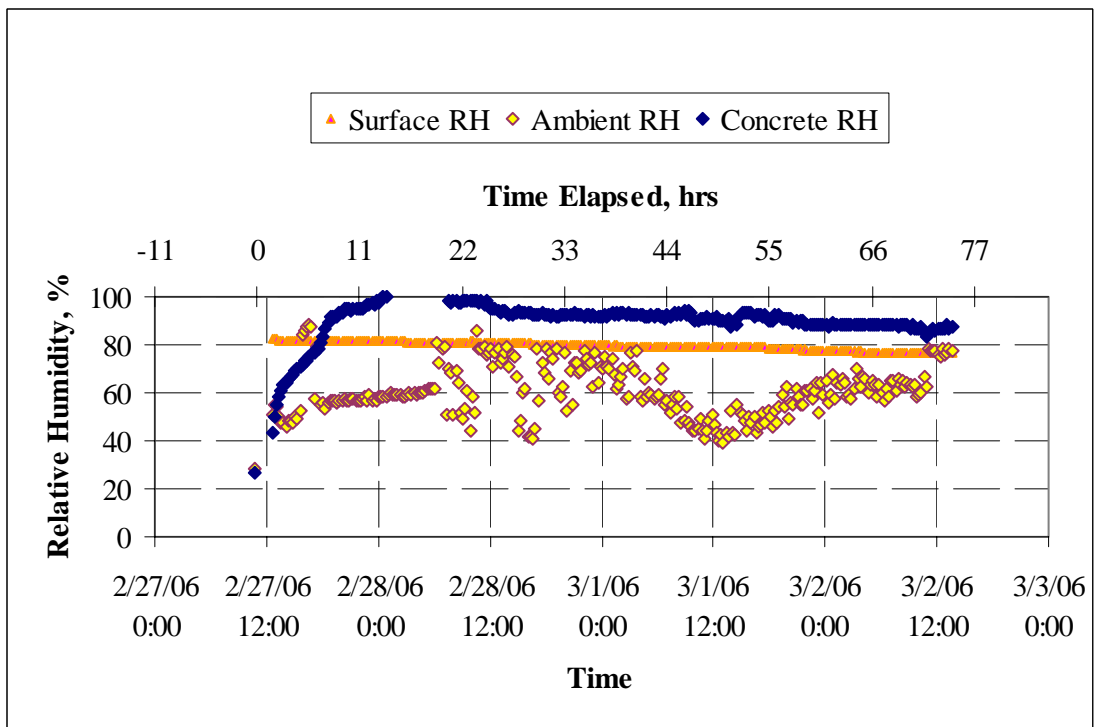
Figure 9 Relative Humidity @ the Lower Layer of Section 1.
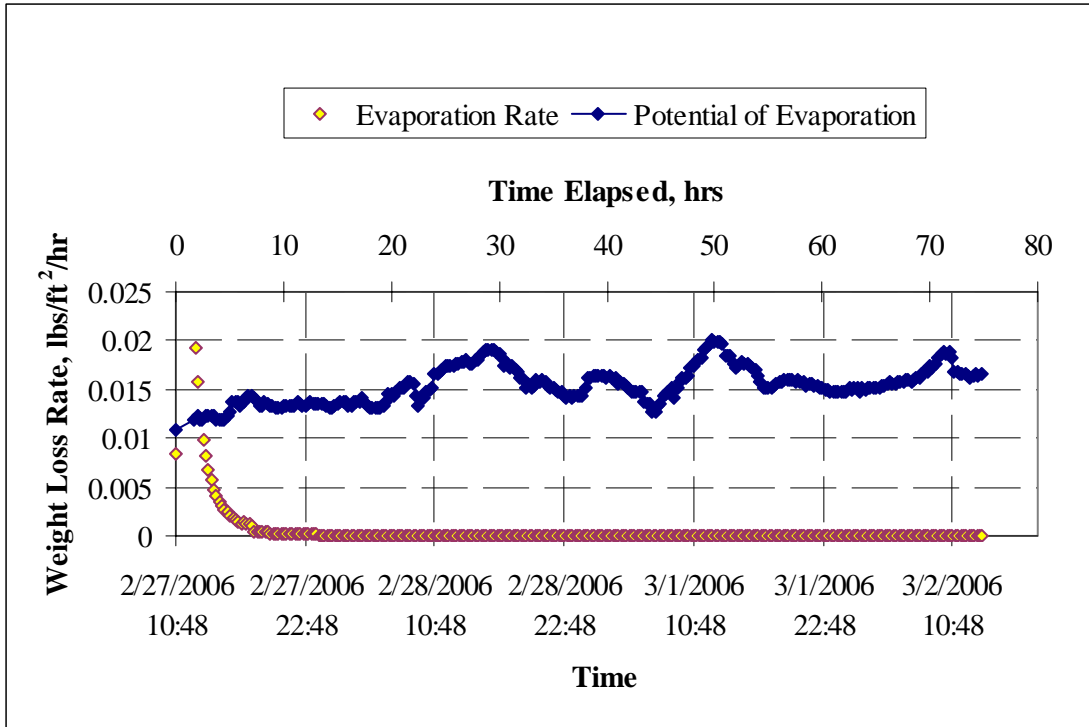
Figure 10 PE and ER @ the Lower Layer of Section 1.
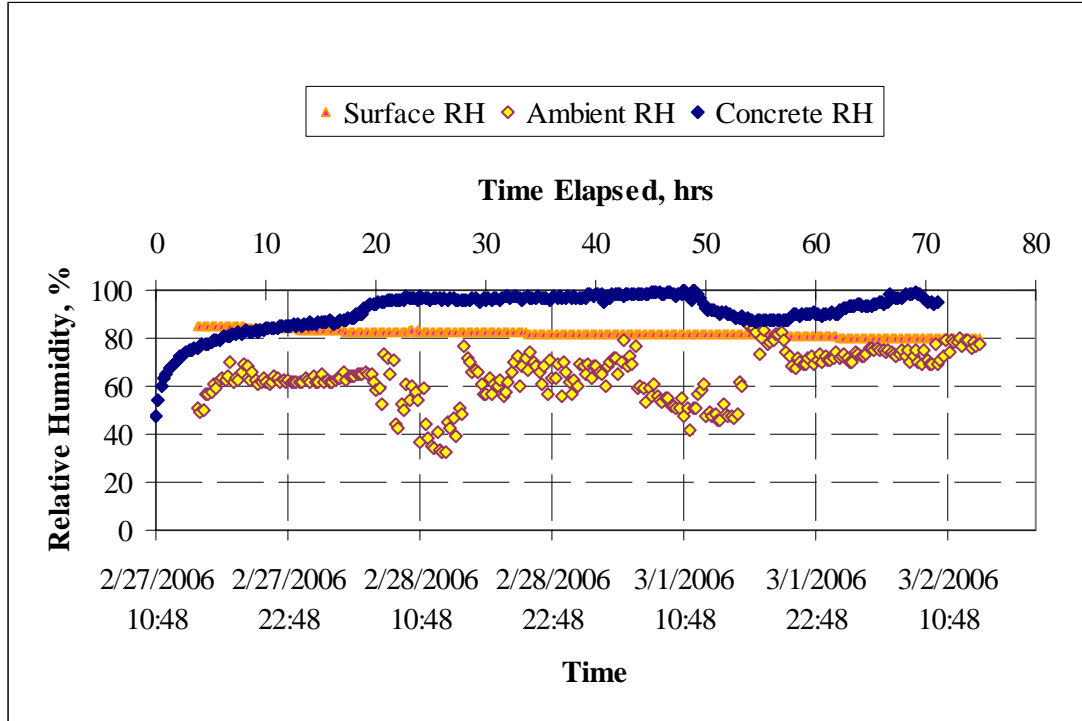
Figure 11 Relative Humidity @ the Lower Layer of Section 2.
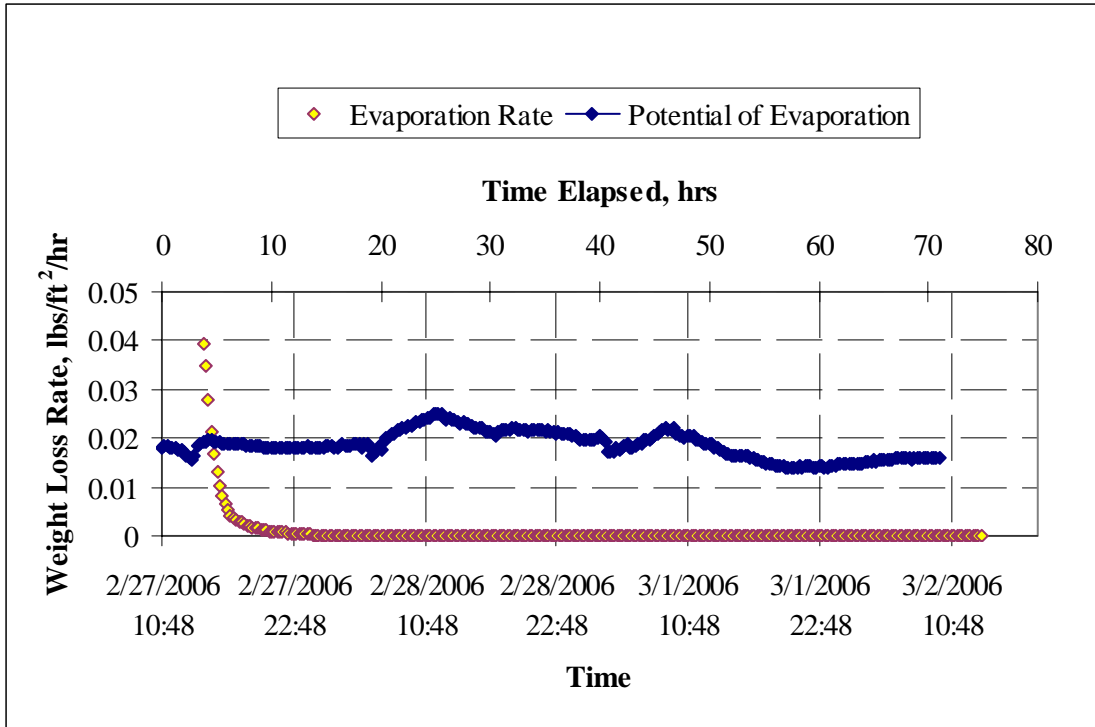
Figure 12 PE and ER @ the Lower Layer of Section 2.
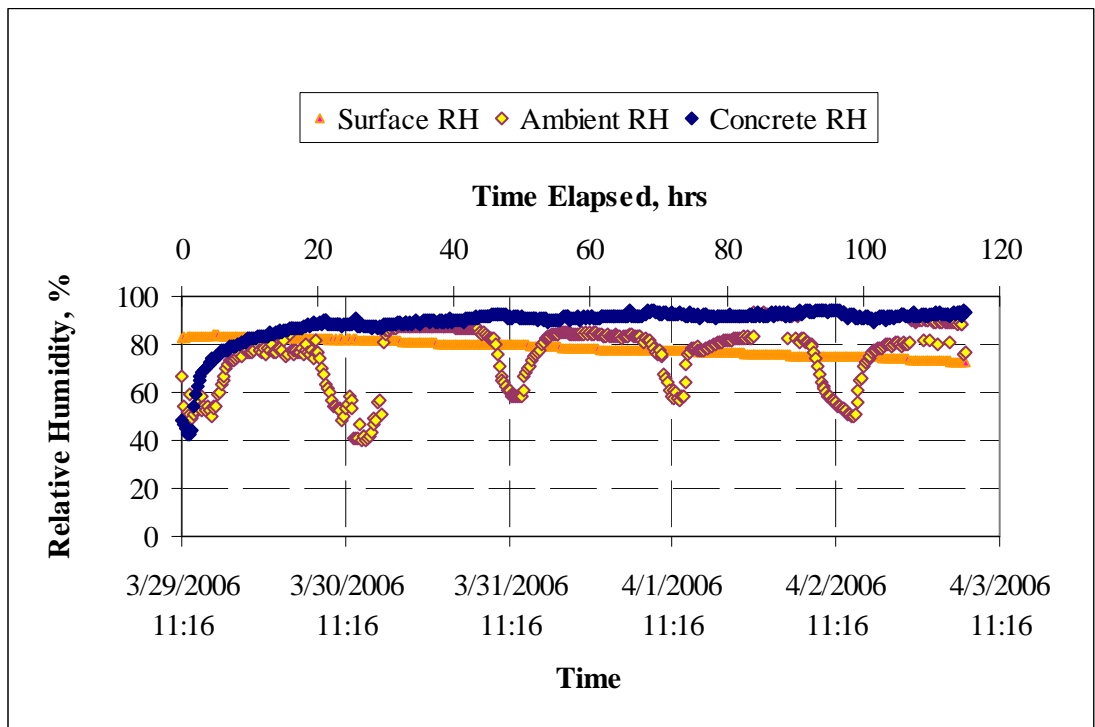
Figure 13 Relative Humidity @ the Upper Layer of Section 1.
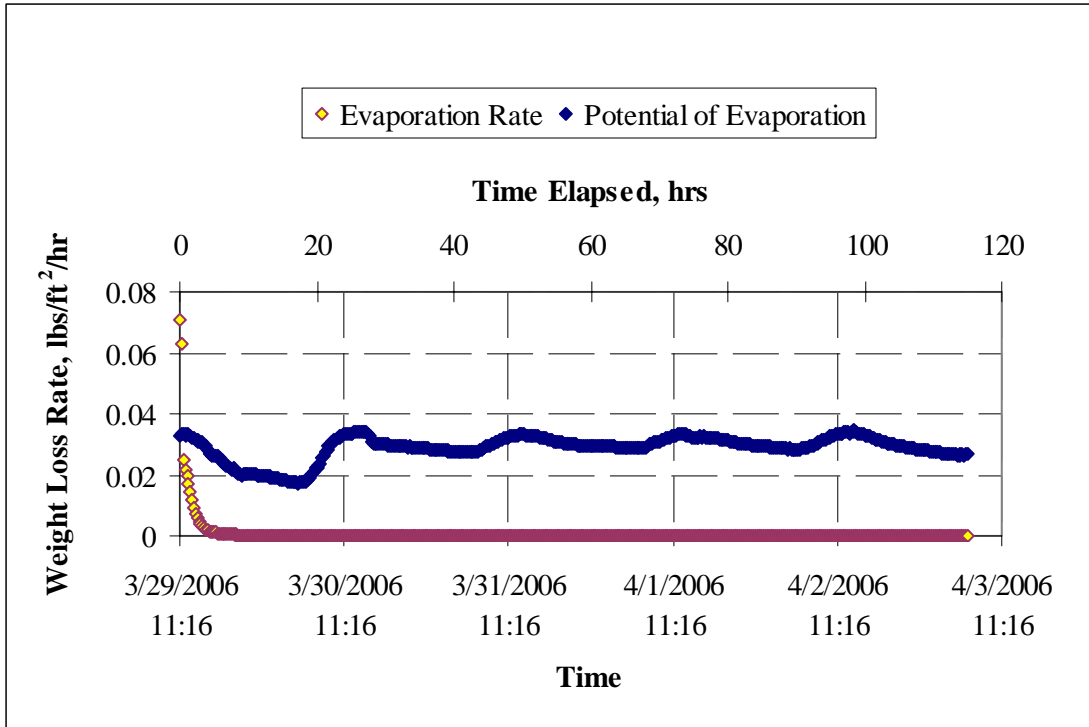
Figure 14 PE and ER @ the Upper Layer of Section 1.
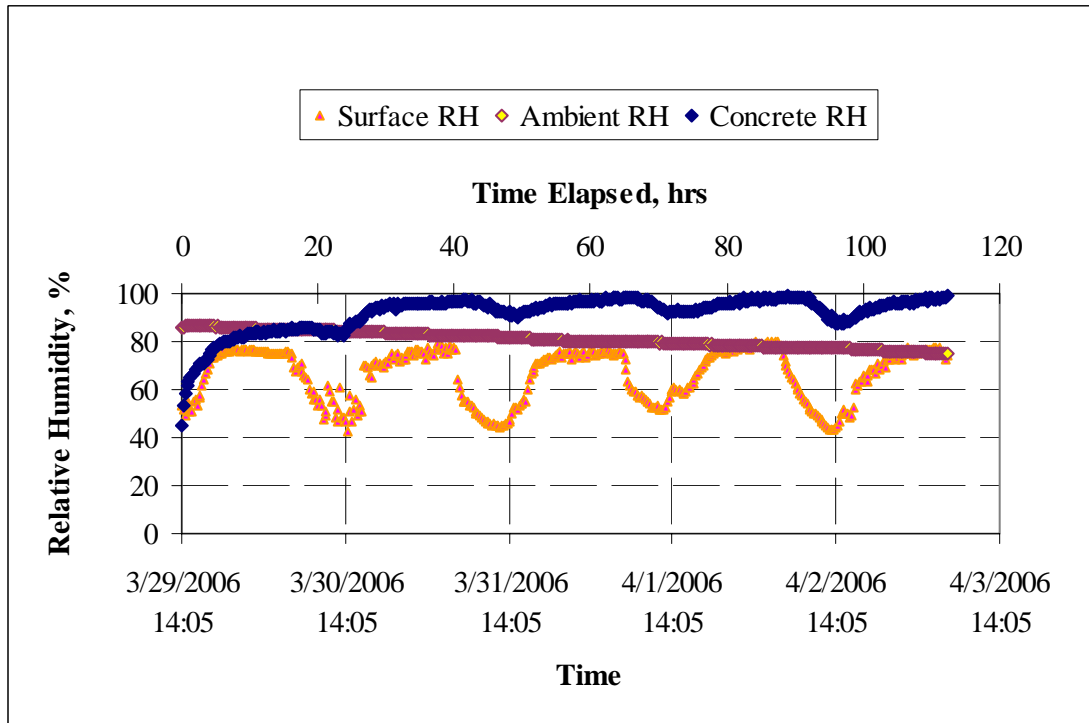
Figure 15 Relative Humidity @ the Upper Layer of Section 2.
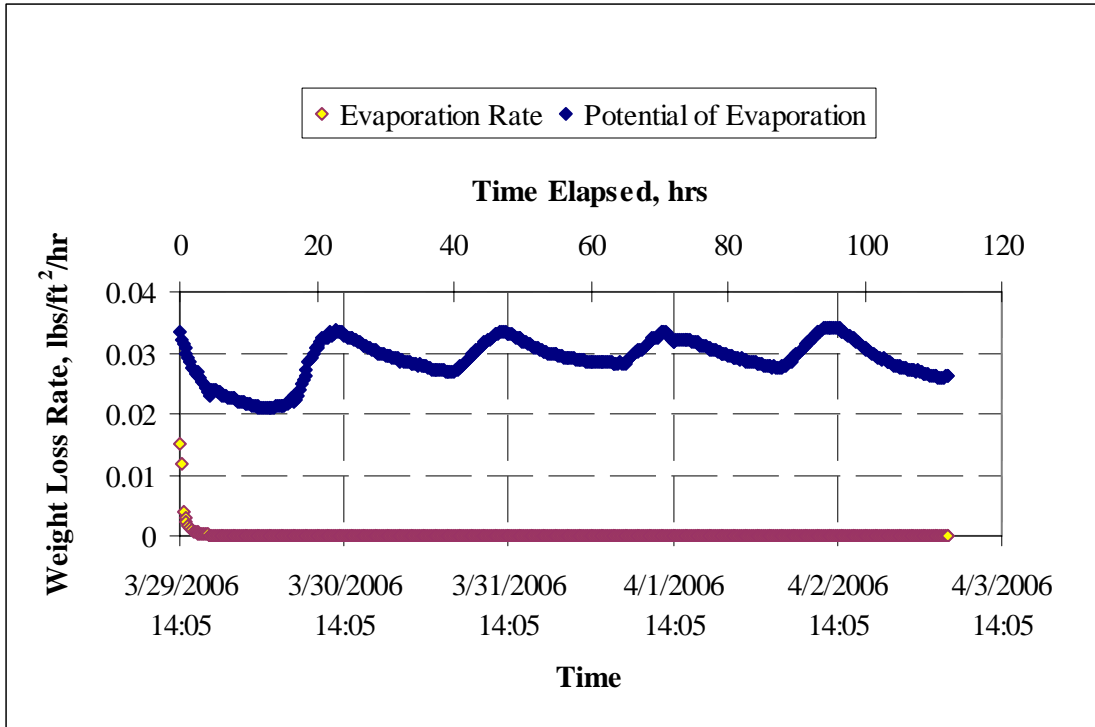
Figure 16 PE and ER @ the Upper Layer of Section 2.
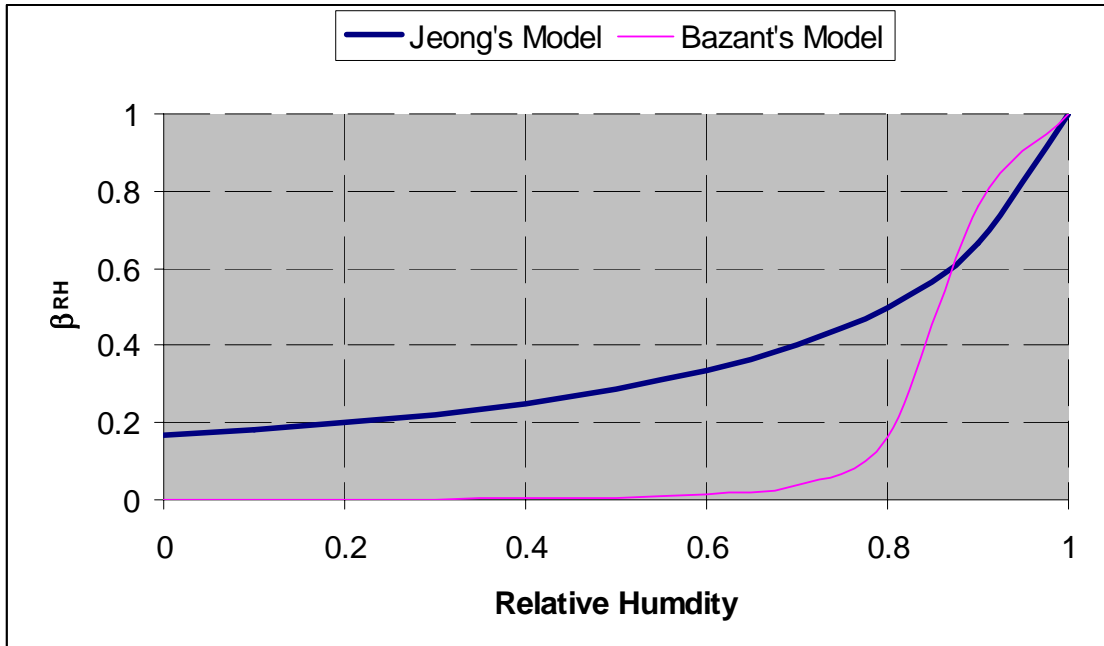
Figure 17 β_{RH} vs. RH.
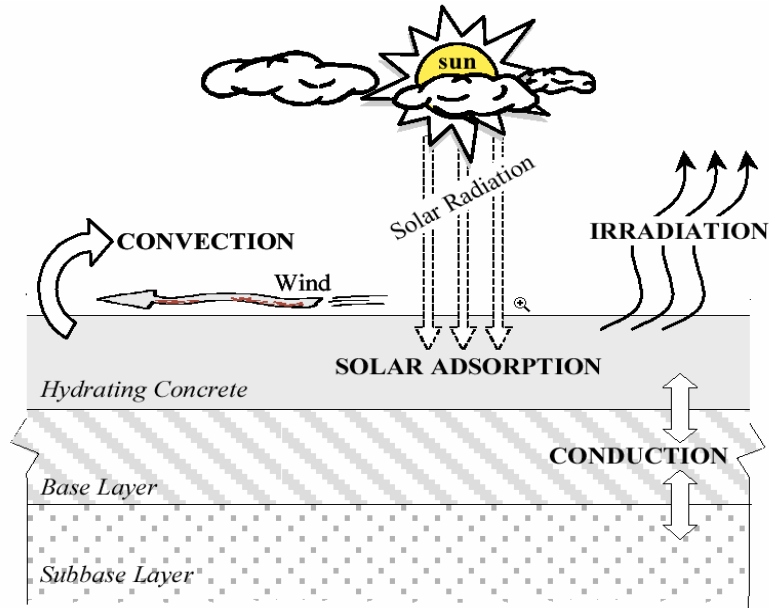
Figure 18 Heat Transfer Mechanisms
between Pavement and its Surroundings. (Ruiz, Schindler et al. 2001)
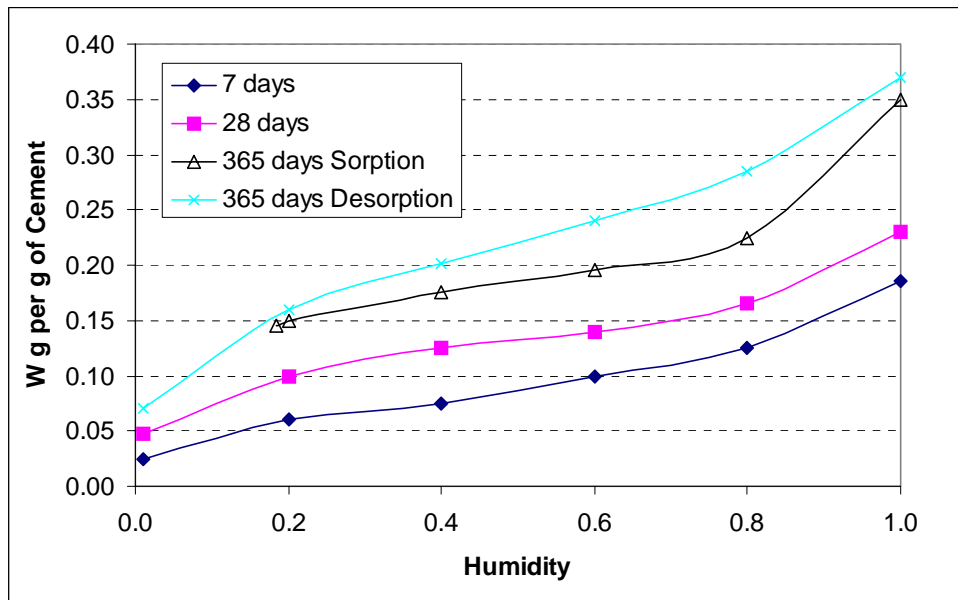
Figure 19 Desorption-Isotherms.

Figure 20 Quadratic Element.
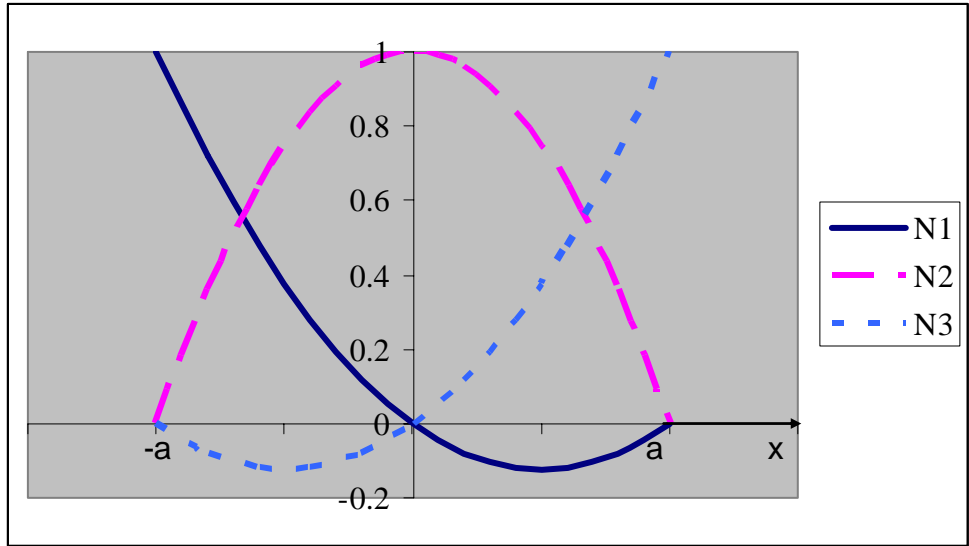
Figure 21 Quadratic Shape Functions.
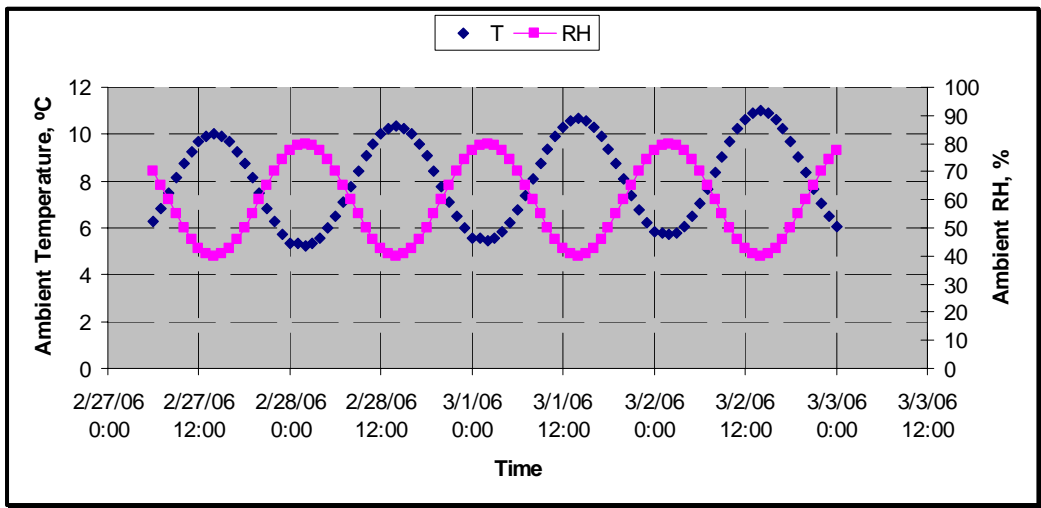
Figure 22 Ambient temperature and relative humidity from 2/27/06 to 3/3/06.
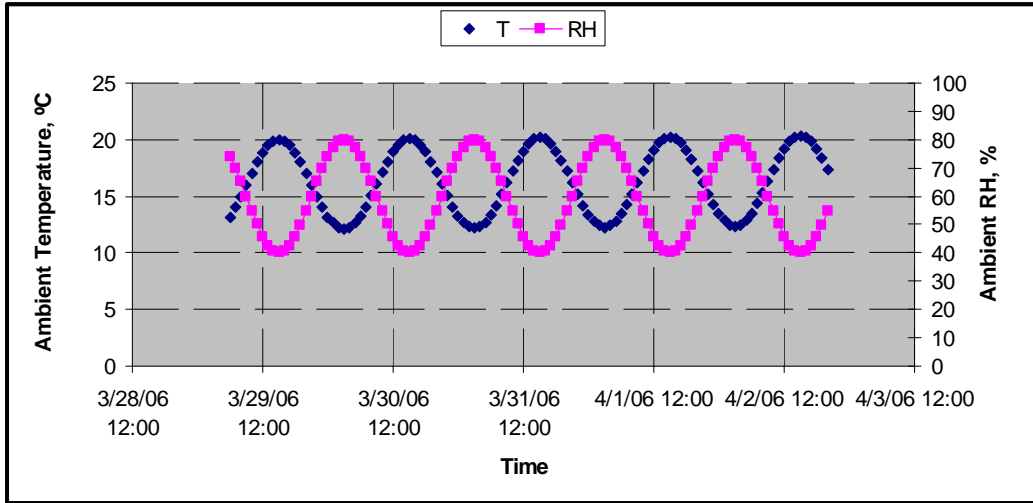
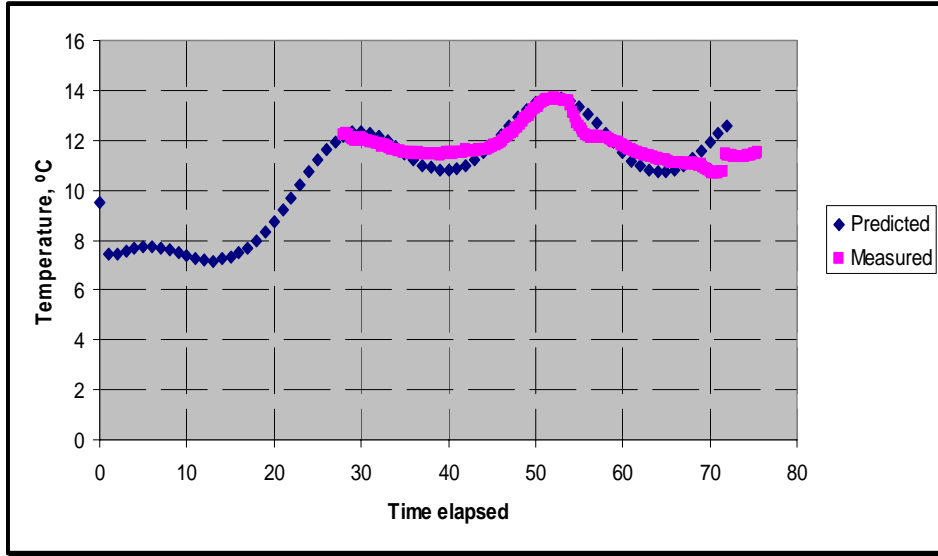**Figure 23** Ambient temperature and relative humidity from 3/28/06 to 4/3/06.
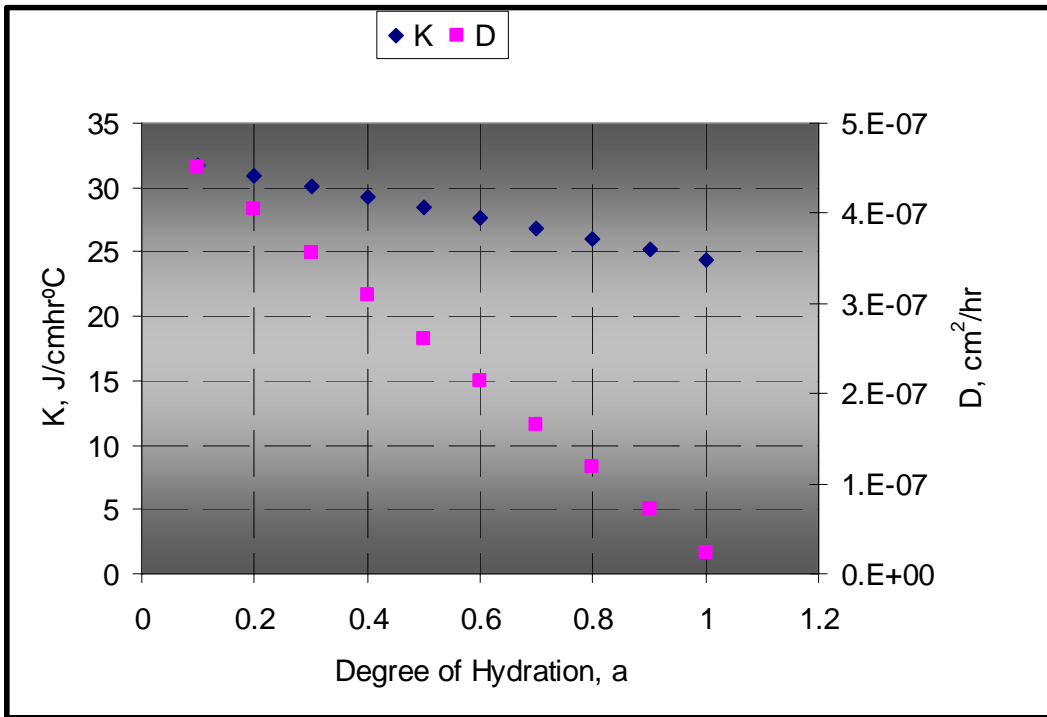
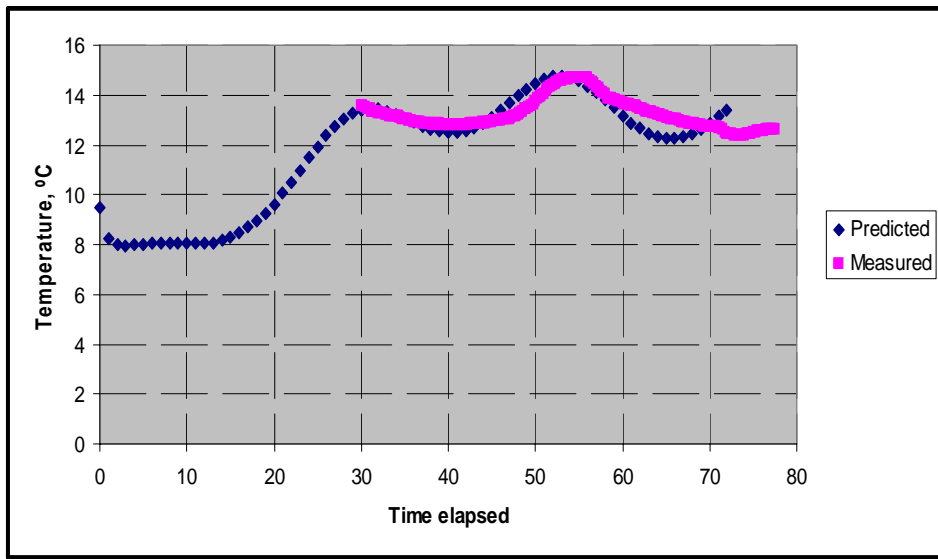
Figure 24 α's effect on K & D. (T=20ºC and RH=0.9)
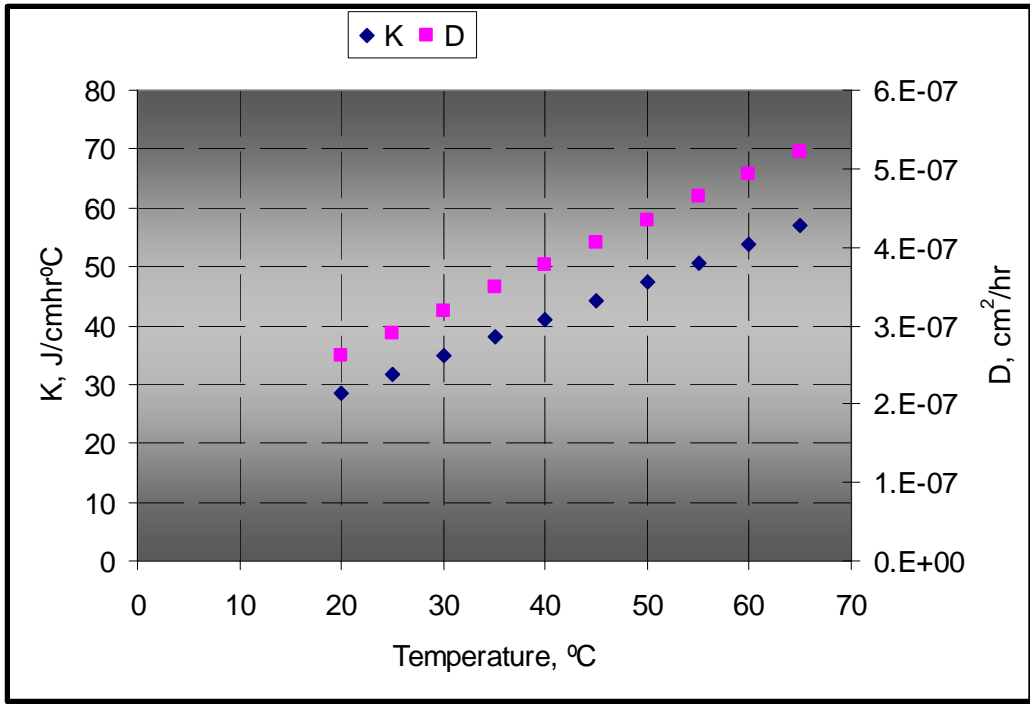
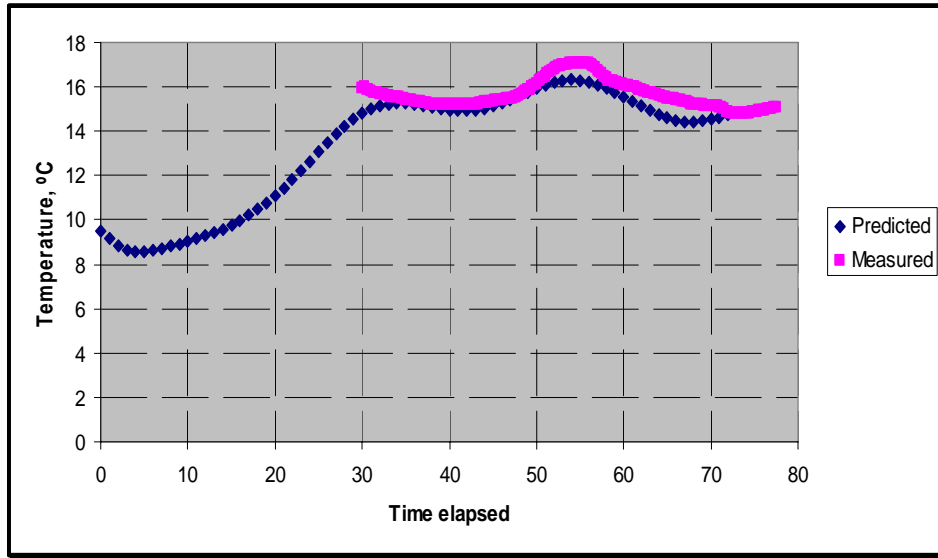**Figure 25** T's effect on K & D. (α=0.5 and RH=0.9)
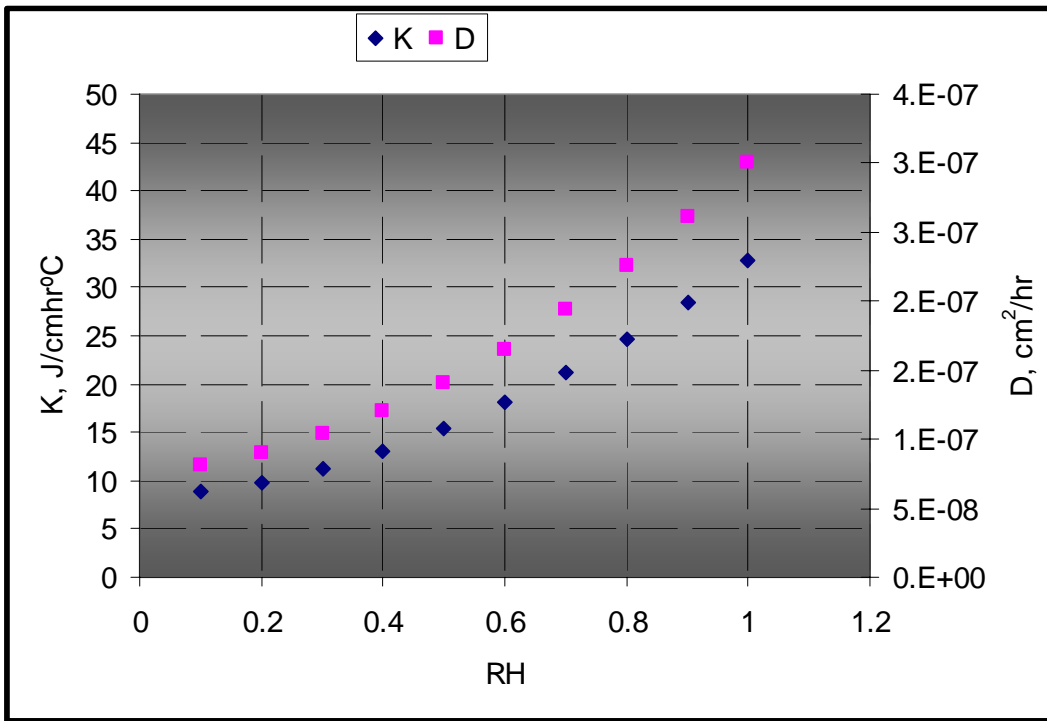
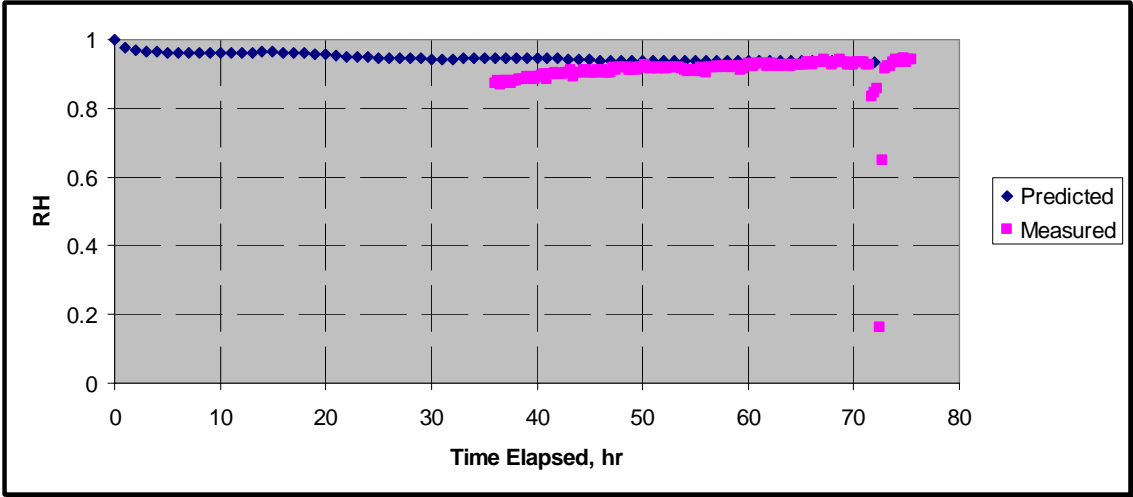**Figure 26** RH's effect on K & D. (α=0.5 and T=20ºC)

Figure 27 Predicted vs. measured temperature history comparison at 1 inch depth.
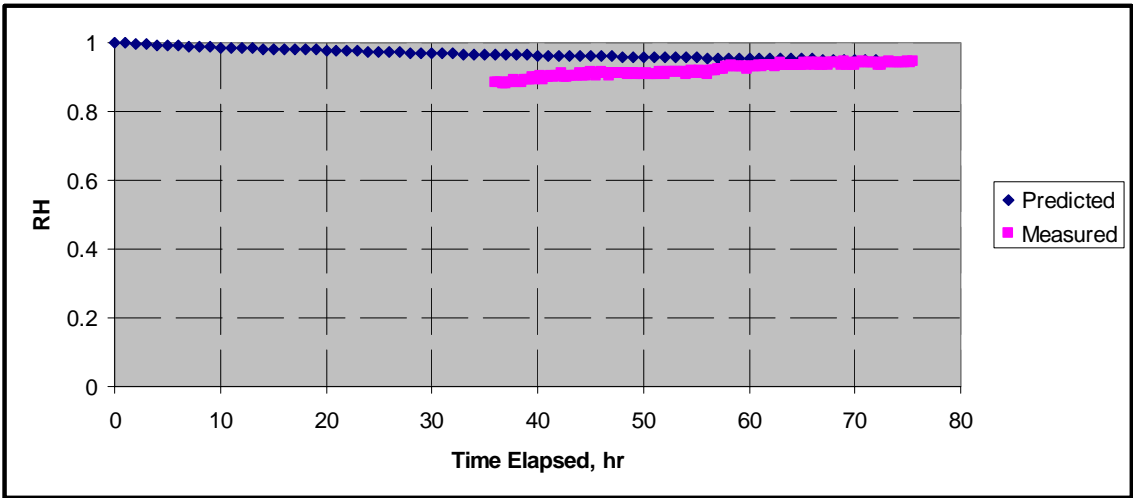

Figure 28 Predicted vs. measured temperature history comparison at 3 inch depth.

Figure 29 Predicted vs. measured temperature history comparison at 7 inch depth.

Figure 30 Predicted vs. measured RH history comparison at 1 inch depth.

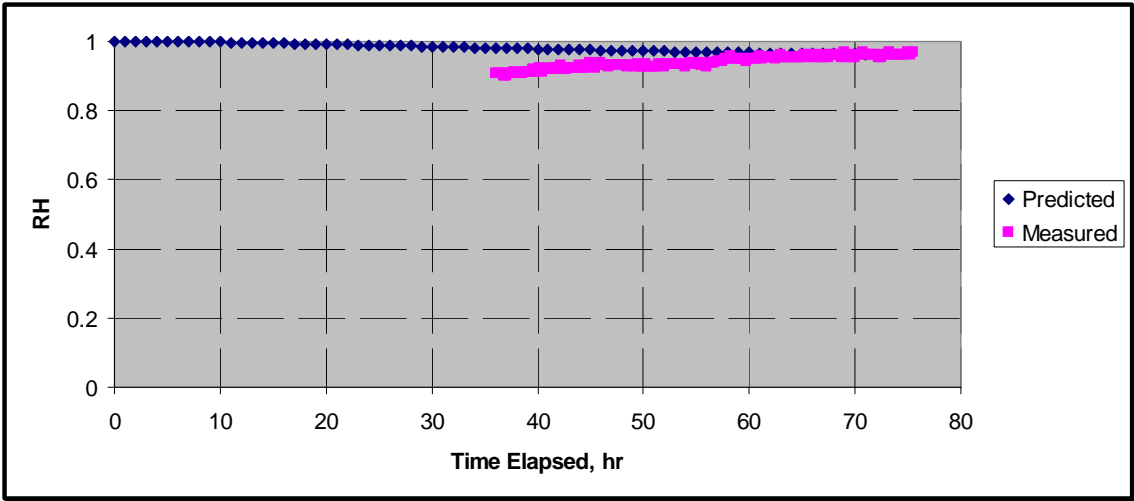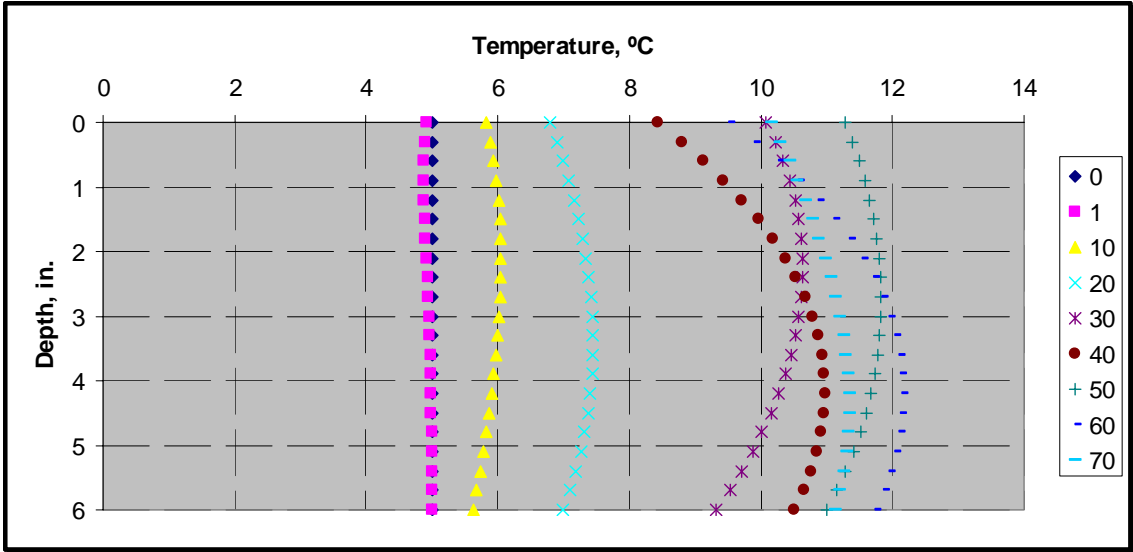**Figure 31** Predicted vs. measured RH history comparison at 3 inch depth.

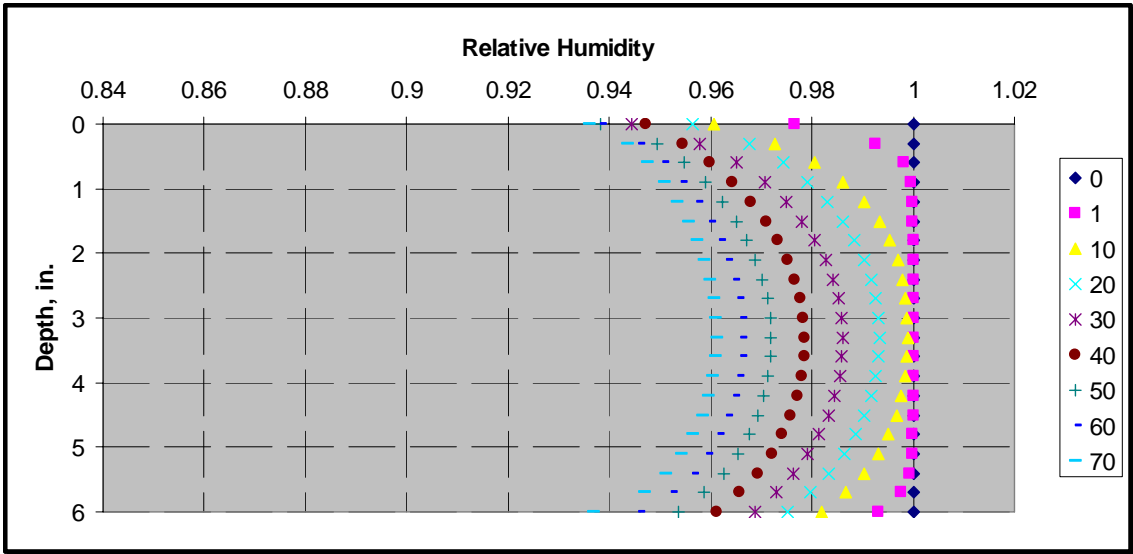**Figure 32** Predicted vs. measured RH history comparison at 7 inch depth.

Figure 33 Section 1 Bottom Layer Temperature Gradients.

Figure 34 Section 1 Bottom Layer RH Gradients.
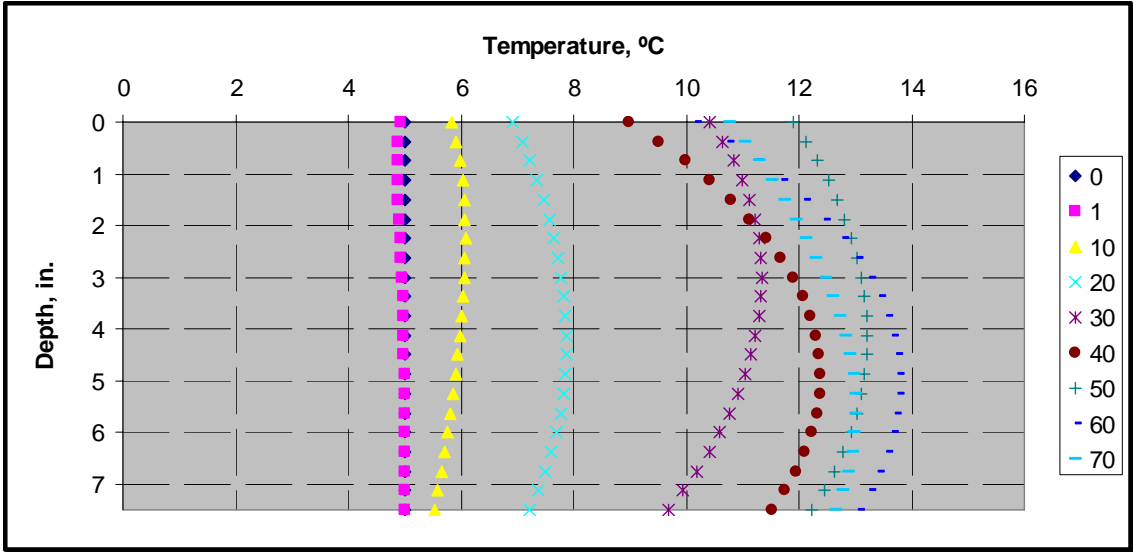
Figure 35 Section 2 Bottom Layer Temperature Gradients.

Figure 36 Section 2 Bottom Layer RH Gradients.

Figure 37 Section 3 Bottom Layer Temperature Gradients.
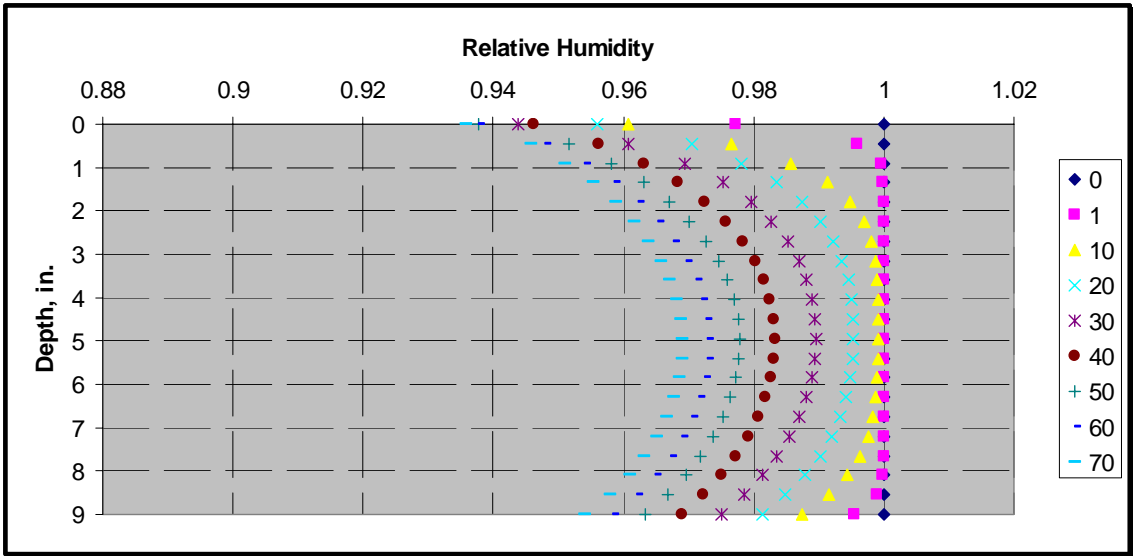
Figure 38 Section 3 Bottom Layer RH Gradients.
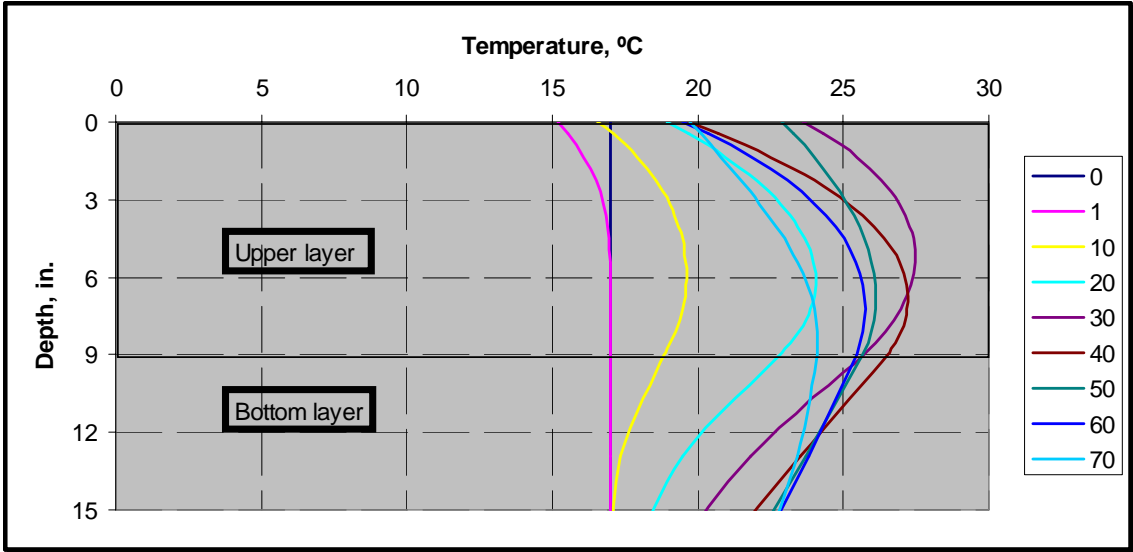
Figure 39 Section 1 Top Layer Temperature Gradients.
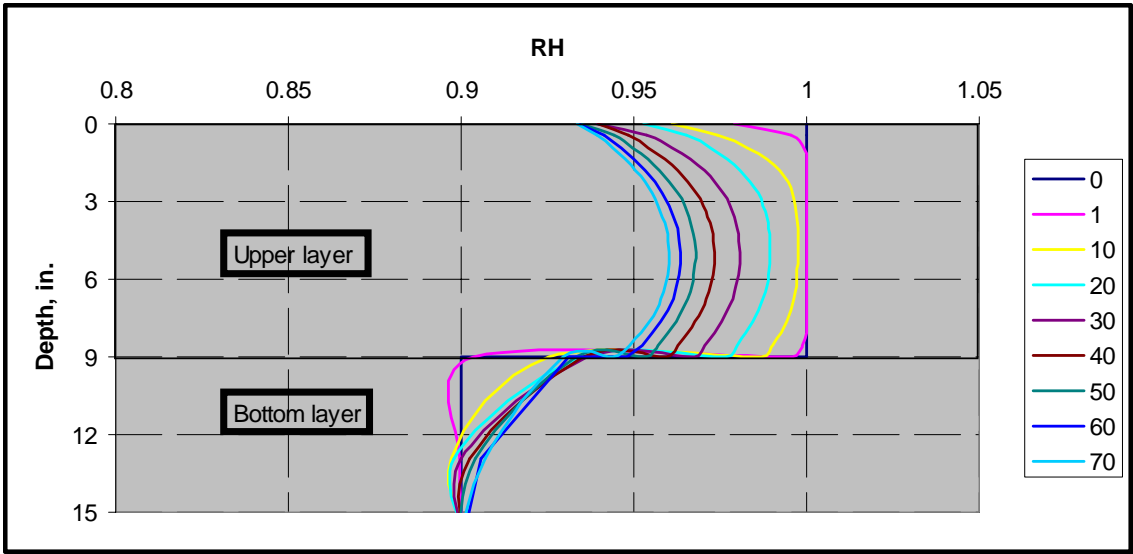
Figure 40 Section 1 Top Layer RH Gradients.
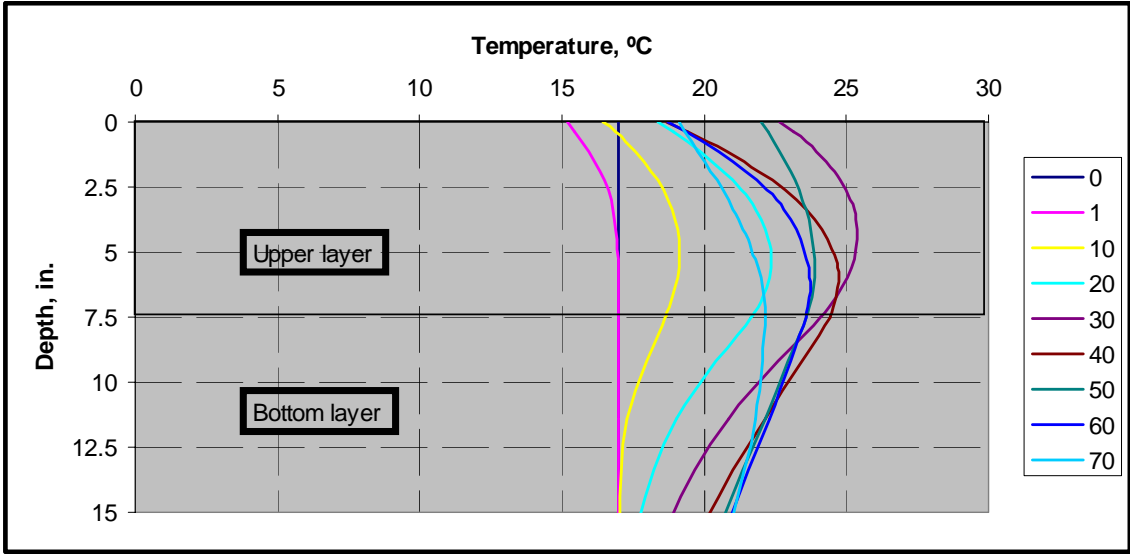
Figure 41 Section 2 Top Layer Temperature Gradients.
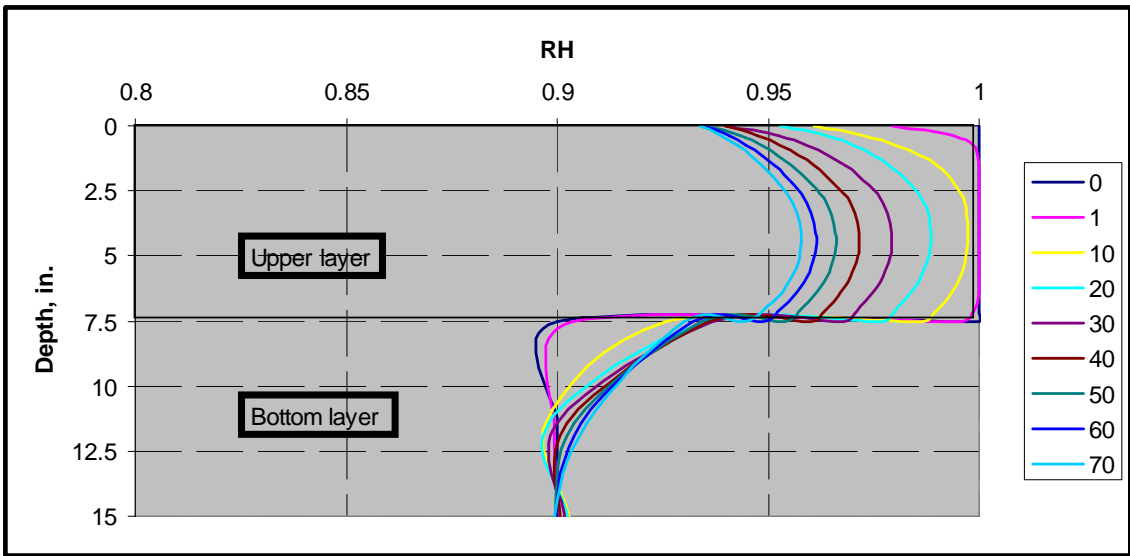
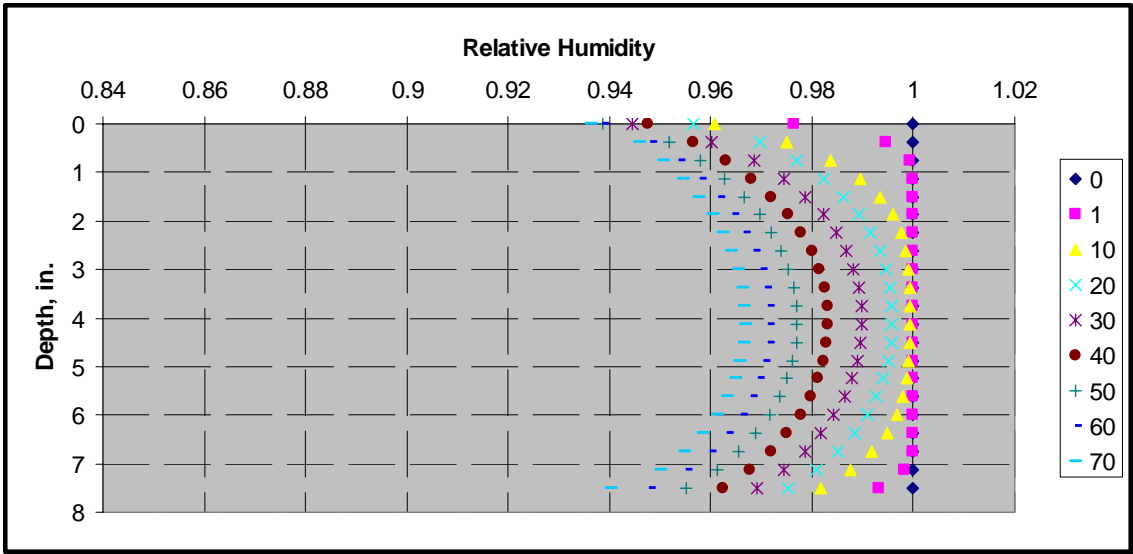**Figure 42** Section 2 Top Layer RH Gradients.

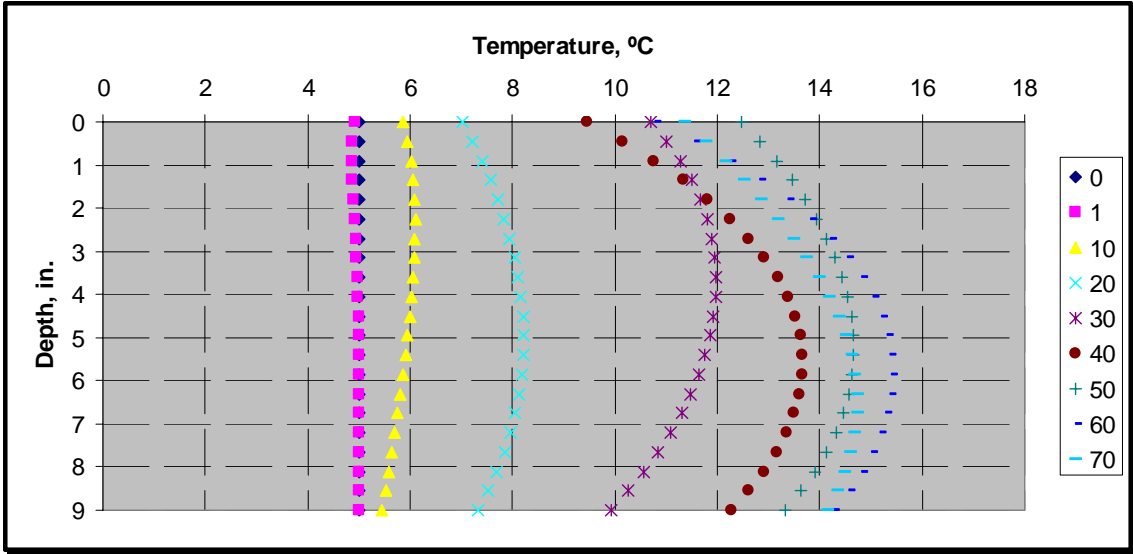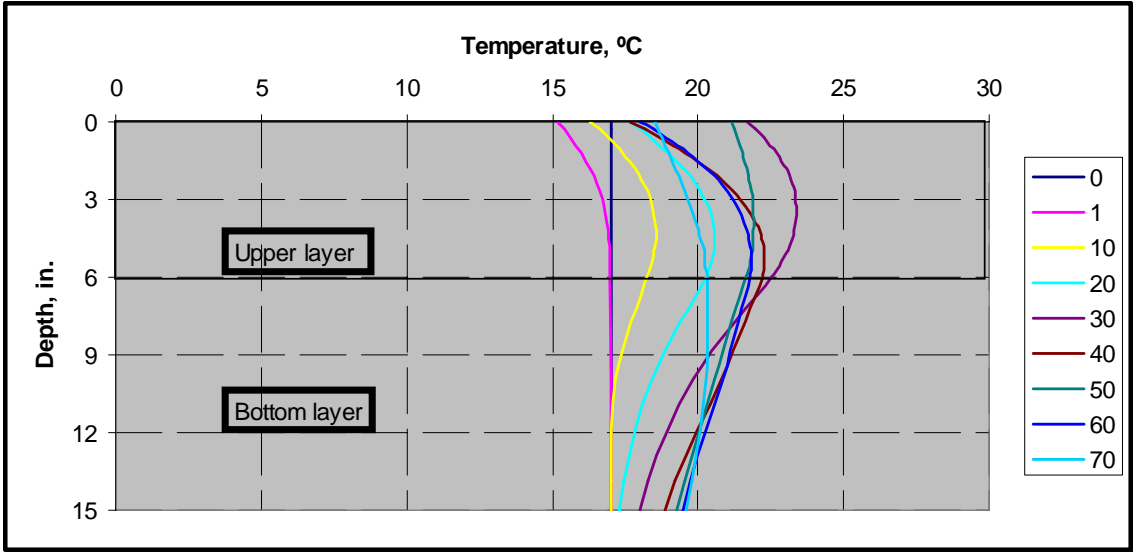**Figure 43** Section 3 Top Layer Temperature Gradients.
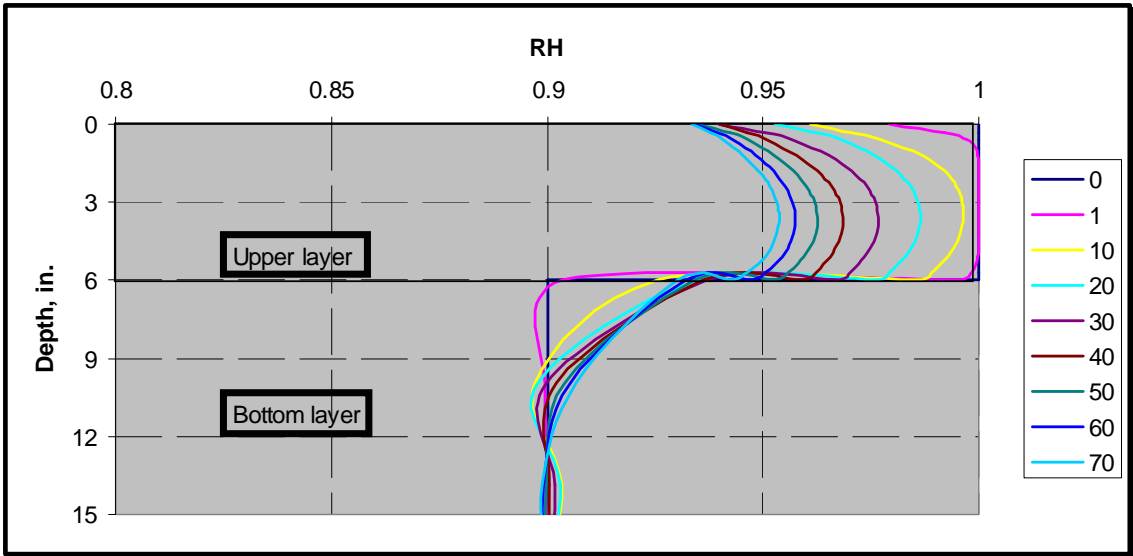
Figure 44 Section 3 Top Layer RH Gradients.
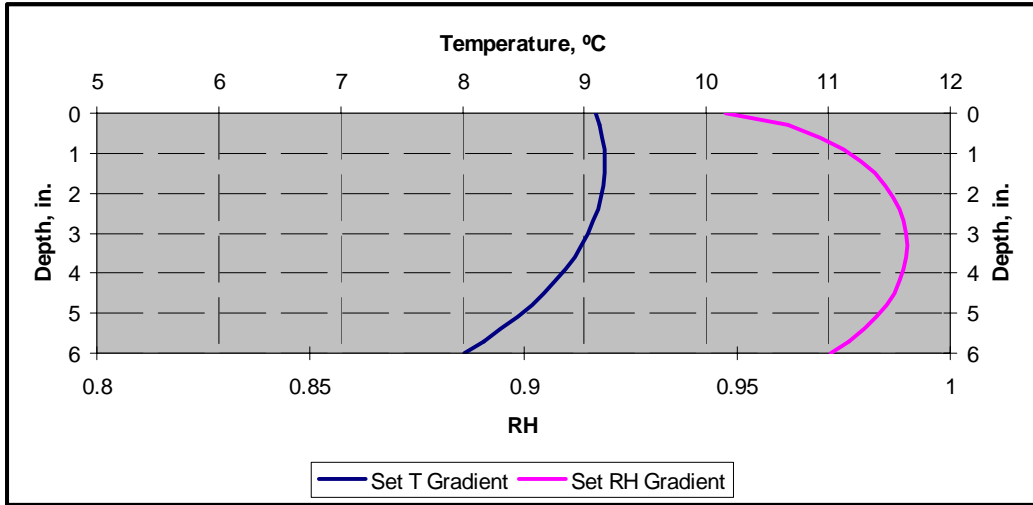
Figure 45 Set T and RH Gradients for the Bottom Layer of Section 1.
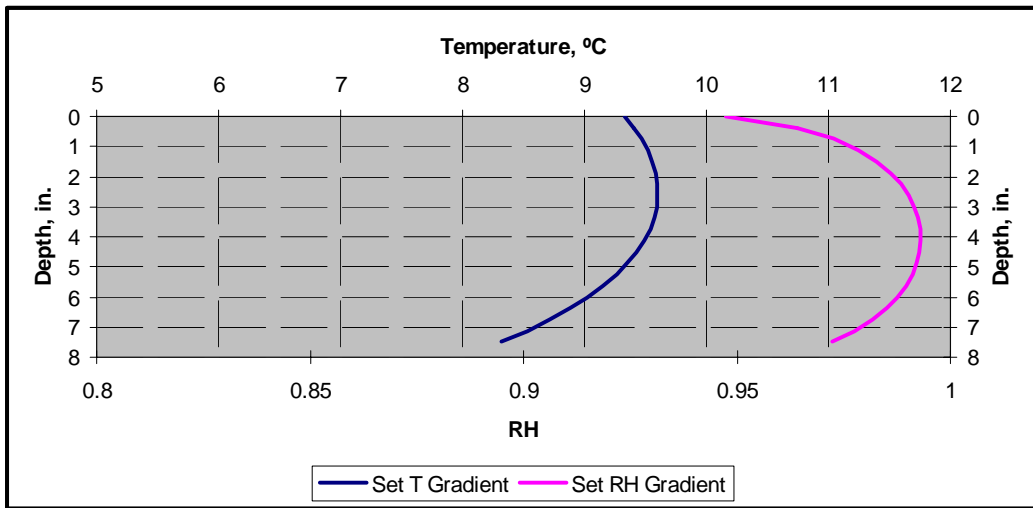
Figure 46 Set T and RH Gradients for the Bottom Layer of Section 2.
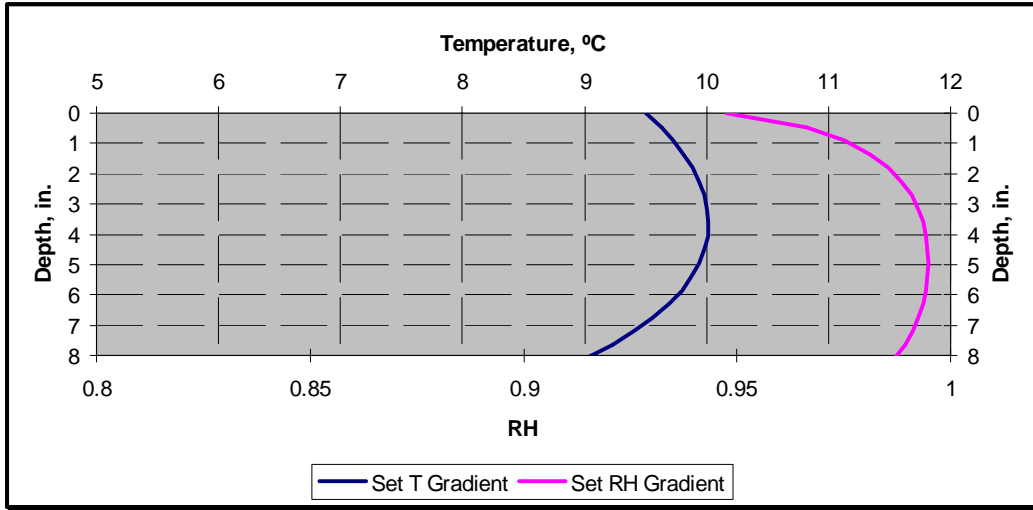
Figure 47 Set T and RH Gradients for the Bottom Layer of Section 3.
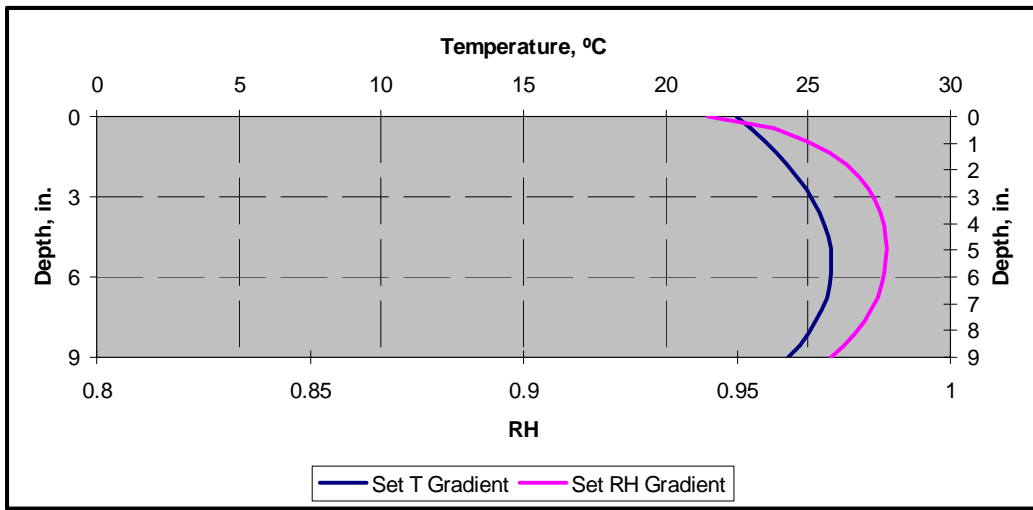
Figure 48 Set T and RH Gradients for the Top Layer of Section 1.
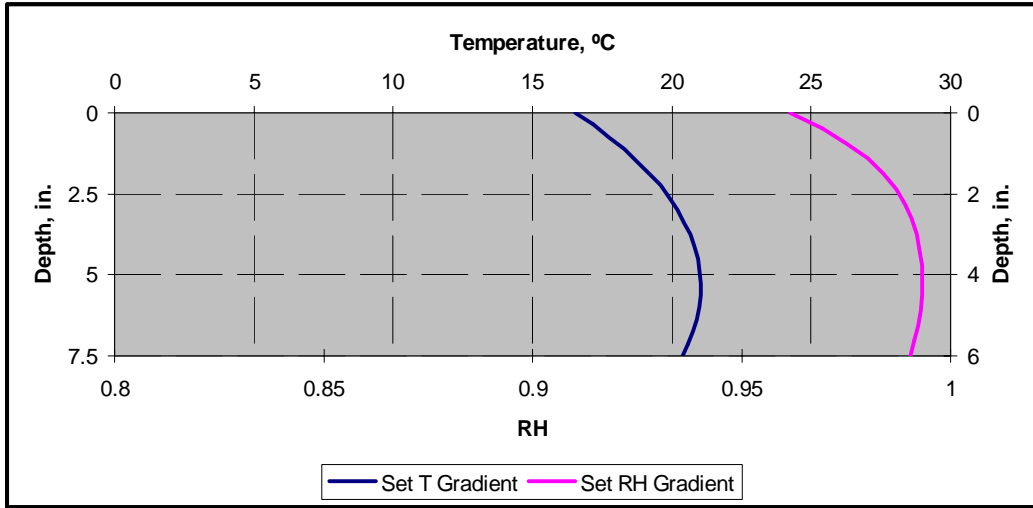
Figure 49 Set T and RH Gradients for the Top Layer of Section 2.
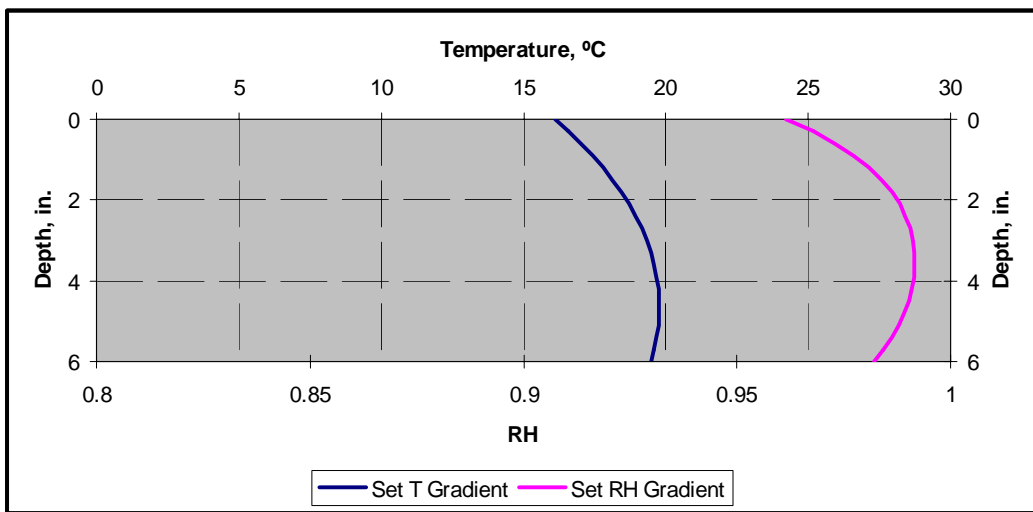
Figure 50 Set T and RH Gradients for the Top Layer of Section 3.

Table 1 Hydration parameters**.**

Total Heat	436.1	J/g
Cement Content	0.32	g/cm^3
Activation Energy	39.184	KJ/mol
Ultimate Hydration, α	0.893	
β	0.785	
τ	37.87	

Table 2 Averaged daily high and low values for temperature and relative humidity.

	2/27 to 3/2		3/29 to 4/3	
	T, ºC	RH, %	T, ºC	RH, %
High	10	85	20	80
Low	5	40	12	40

Table 3 Calibrated coefficients.

a	196.000
b	49.000
c	10.808
d	10.294

Table 4 Equivalent Linear Temperature and Moisture Gradients for Section 1 Bottom Layer.

Time, hours	Temperature						Moisture					
	A	B	C	D	ΔT, °C/in	ΔT, °C/cm	A	B	C	D	ΔRH, 1/in	ΔRH, 1/cm
Set Gradient	9.033700	-0.161600	-0.052800	-0.001900	1.031160	0.405969	0.990901	0.000522	-0.003112	0.000351	-0.014504	-0.005710
10	6.018024	-0.061339	-0.032078	0.003026	0.269992	0.106296	1.000461	0.000222	-0.002900	0.000348	-0.012607	-0.004963
20	7.437321	0.050482	-0.060568	-0.002016	-0.237574	-0.093533	0.994184	0.000766	-0.002890	0.000235	-0.012210	-0.004807
30	10.579648	-0.147207	-0.097313	0.002660	0.797058	0.313802	0.986942	0.000781	-0.003061	0.000321	-0.015086	-0.005940
40	10.786489	0.330352	-0.145647	0.001823	-2.041177	-0.803613	0.978896	0.001415	-0.002604	0.000098	-0.011665	-0.004593
50	11.820086	-0.033169	-0.074651	-0.001458	0.246253	0.096950	0.972694	0.000936	-0.002678	0.000150	-0.010476	-0.004124
60	11.954198	0.325572	-0.147228	0.004880	-2.111544	-0.831317	0.966672	0.001184	-0.002495	0.000004	-0.007234	-0.002848
70	11.198402	0.194603	-0.061510	-0.003888	-1.041647	-0.410097	0.962066	0.001228	-0.002489	-0.000105	-0.003966	-0.001561

Table 5 Equivalent Linear Temperature and Moisture Gradients for Section 1 Upper Layer.

Time, hours	Temperature						Moisture					
	A	B	C	D	ΔT, °C/in	ΔT, °C/cm	A	B	C	D	ΔRH, 1/in	ΔRH, 1/cm
Set Gradient	25.708476	0.235120	-0.114006	-0.001440	-1.958616	-0.771109	0.986293	0.000054	-0.001244	0.000139	-0.015686	-0.006175
10	19.480021	0.211459	-0.086277	0.002123	-2.135281	-0.840662	0.999589	-0.000438	-0.001080	0.000154	-0.012898	-0.005078
20	23.680763	0.448799	-0.136751	-0.000883	-3.942635	-1.552218	0.990668	0.000122	-0.001137	0.000115	-0.013673	-0.005383
30	27.409596	0.177998	-0.134356	0.002486	-1.873826	-0.737727	0.981682	0.000312	-0.001245	0.000124	-0.016367	-0.006444
40	26.425459	0.699400	-0.163721	0.003191	-6.643536	-2.615565	0.973685	0.000800	-0.001123	0.000066	-0.014417	-0.005676
50	25.721084	0.343720	-0.070658	-0.001567	-2.922129	-1.150444	0.968280	0.000802	-0.001115	0.000056	-0.013342	-0.005253
60	25.029909	0.563323	-0.126040	0.005090	-5.626499	-2.215157	0.963764	0.001012	-0.001055	0.000024	-0.011732	-0.004619
70	22.957937	0.550149	-0.051445	-0.003194	-4.602077	-1.811841	0.960434	0.001071	-0.001017	0.000004	-0.010076	-0.003967

Table 6 Equivalent Linear Temperature and Moisture Gradients for Section 2 Bottom Layer.

Time, hours	Temperature						Moisture					
	A	B	C	D	ΔT, °C/in	ΔT, °C/cm	A	B	C	D	ΔRH, 1/in	ΔRH, 1/cm
Set Gradient	9.542299	-0.108712	-0.050505	-0.001894	0.935195	0.368187	0.994502	0.000055	-0.002168	0.000202	-0.013195	-0.005195
10	6.018056	0.077986	-0.022945	0.002550	-0.746262	-0.293804	1.001871	-0.000312	-0.001850	0.000209	-0.010886	-0.004286
20	7.859059	0.058878	-0.055909	-0.001544	-0.343879	-0.135385	0.997148	0.000253	-0.001987	0.000144	-0.011010	-0.004335
30	11.297613	-0.128431	-0.087684	0.002146	0.827431	0.325760	0.991119	0.000265	-0.002174	0.000189	-0.013948	-0.005491
40	12.210912	0.308771	-0.139137	0.002086	-2.447787	-0.963696	0.983793	0.000890	-0.001927	0.000072	-0.011231	-0.004422
50	13.202976	0.062814	-0.080419	-0.001495	-0.376500	-0.148228	0.978001	0.000579	-0.001987	0.000098	-0.010544	-0.004151
60	13.574483	0.320648	-0.138751	0.004593	-2.695511	-1.061225	0.972290	0.000857	-0.001874	0.000023	-0.007883	-0.003104
70	12.732040	0.295005	-0.072214	-0.003111	-2.015670	-0.793571	0.967824	0.000891	-0.001858	-0.000025	-0.005100	-0.002008

Table 7 Equivalent Linear Temperature and Moisture Gradients for Section 2 Upper Layer.

Time, hours	Temperature						Moisture					
	A	B	C	D	ΔT, °C/in	ΔT, °C/cm	A	B	C	D	ΔRH, 1/in	ΔRH, 1/cm
Set Gradient	20.653186	0.480246	-0.155264	0.002228	-3.742836	-1.473557	0.993832	0.000721	-0.001482	0.000139	-0.014204	-0.005592
10	18.978431	0.249278	-0.101588	0.002577	-2.032661	-0.800260	0.998754	-0.000036	-0.001572	0.000237	-0.014728	-0.005798
20	22.007083	0.456357	-0.140960	-0.001200	-3.346740	-1.317614	0.989212	0.000636	-0.001572	0.000168	-0.015401	-0.006063
30	25.347291	0.149589	-0.138005	0.002996	-1.311508	-0.516342	0.979914	0.000855	-0.001678	0.000188	-0.018309	-0.007208
40	23.892763	0.725539	-0.167069	0.003075	-5.636132	-2.218950	0.971715	0.001350	-0.001464	0.000091	-0.015884	-0.006253
50	23.673903	0.235416	-0.061990	-0.001646	-1.661459	-0.654118	0.966122	0.001261	-0.001436	0.000081	-0.014583	-0.005741
60	23.039256	0.569539	-0.134113	0.005609	-4.626487	-1.821452	0.961328	0.001433	-0.001330	0.000031	-0.012709	-0.005004
70	21.211654	0.460348	-0.041286	-0.004014	-3.198599	-1.259291	0.957800	0.001432	-0.001266	0.000001	-0.010803	-0.004253

Table 8 Equivalent Linear Temperature and Moisture Gradients for Section 3 Bottom Layer.

Time, hours	Temperature						Moisture					
	A	B	C	D	ΔT, °C/in	ΔT, °C/cm	A	B	C	D	ΔRH, 1/in	ΔRH, 1/cm
Set Gradient	13.738056	0.239902	-0.079101	-0.001765	-1.966115	-0.774061	0.994245	-0.000290	-0.001348	0.000166	-0.015542	-0.006119
10	9.647213	0.248842	-0.049086	0.001479	-2.401307	-0.945396	1.001724	-0.000693	-0.001115	0.000168	-0.012134	-0.004777
20	12.024298	0.377481	-0.084944	-0.001210	-3.265016	-1.285439	0.996914	-0.000159	-0.001218	0.000134	-0.013222	-0.005205
30	15.479632	0.184493	-0.104614	0.001671	-1.843161	-0.725654	0.990926	-0.000072	-0.001362	0.000158	-0.016629	-0.006547
40	16.418013	0.529377	-0.146020	0.002786	-5.069042	-1.995686	0.983907	0.000568	-0.001215	0.000092	-0.015172	-0.005973
50	16.847553	0.350312	-0.090713	-0.000797	-3.065656	-1.206951	0.978518	0.000448	-0.001246	0.000105	-0.015514	-0.006108
60	16.903467	0.503962	-0.131759	0.004644	-5.043479	-1.985622	0.987342	0.000729	-0.001158	0.000070	-0.014216	-0.005597
70	15.710982	0.529392	-0.078012	-0.001798	-4.567917	-1.798392	0.969421	0.000766	-0.001115	0.000055	-0.012908	-0.005082

Table 9 Equivalent Linear Temperature and Moisture Gradients for Section 3 Upper Layer.

Time, hours	Temperature						Moisture					
	A	B	C	D	ΔT, °C/in	ΔT, °C/cm	A	B	C	D	ΔRH, 1/in	ΔRH, 1/cm
Set Gradient	19.331327	0.539077	-0.170839	0.002497	-3.315365	-1.305262	0.991557	0.001662	-0.002131	0.000191	-0.016160	-0.006362
10	18.365736	0.296281	-0.119703	0.003065	-1.876992	-0.738973	0.997147	0.000804	-0.002394	0.000375	-0.016974	-0.006683
20	20.235695	0.446877	-0.142203	-0.001541	-2.631334	-1.035958	0.986581	0.001441	-0.002219	0.000263	-0.017167	-0.006759
30	23.363454	0.107269	-0.141474	0.003516	-0.757532	-0.298241	0.976705	0.001656	-0.002316	0.000306	-0.019850	-0.007815
40	21.456141	0.737773	-0.169080	0.002770	-4.516386	-1.778105	0.968184	0.002088	-0.001940	0.001280	-0.054000	-0.021260
50	21.865600	0.095887	-0.052430	-0.001404	-0.529832	-0.208595	0.962324	0.001832	-0.001881	0.000121	-0.014912	-0.005871
60	21.189169	0.580638	-0.144056	0.005920	-3.675636	-1.447101	0.957215	0.001914	-0.001699	0.000031	-0.012488	-0.004917
70	19.663757	0.339655	-0.028658	-0.004618	-1.888307	-0.743428	0.953486	0.001829	-0.001597	-0.000028	-0.010067	-0.003963